Pergamon

Int. J. Solids Structures Vol. 34, No. 2, pp. 243–274, 1997

0020–7683/97 $15.00 + .00

PII: S0020–7683(96)00006–6

ON SOLUTIONS OF TWO-DIMENSIONAL LINEAR ELASTOSTATIC AND HEAT-TRANSFER PROBLEMS IN THE VICINITY OF SINGULAR POINTS

ZOHAR YOSIBASH†
Pearlstone Center for Aeronautical Engineering Studies, Dept. of Mechanical Engineering, Ben-Gurion University of the Negev, Beer-Sheva 84105, Israel

(*Received* 26 *January* 1995; *in revised form* 6 *December* 1995)

Abstract—Singular points associated with the linear theories of steady-state heat transfer and elasticity are discussed. Exact solutions for a set of benchmark problems consisting of crack tips, wedge corners of different angles and materials and internal multi-material interfaces in isotropic as well as anisotropic materials are provided and described in detail. Both the generalized flux/stress intensity factors (GFIFs/GSIFs) and the eigenfunctions are explicitly presented. The efficiency, robustness and accuracy of new numerical methods based on the p-version of the finite element method are demonstrated on the basis of the benchmark problems. Copyright © 1996 Elsevier Science Ltd.

1. INTRODUCTION

The solutions of linear elastostatic and steady-state heat transfer problems in the vicinity of crack tips were an intensive subject of research during the last 30 years. Although an exact solution can be obtained for cracks in bodies of simple geometries, for most cases involving complex geometries, anisotropic materials, and cracks at bi-material interfaces, only a numerical approximated solution can be obtained. Some typical singular points in an electronic device, for example, where failure initiation commonly occurs, are illustrated in Fig. 1. The solution in the vicinity of singular points is of considerable engineering interest (especially for general domains containing multi-material interfaces, and anisotropic materials) because it is directly or indirectly related to failure initiation in composite materials and electronic devices.

The exact solution for linear elastostatic problems in two dimensions, for example, in the vicinity of any singular point can be expressed in the following form (Williams 1952, Dempsey and Sinclair 1979, Gregory 1979, Dempsey 1995):

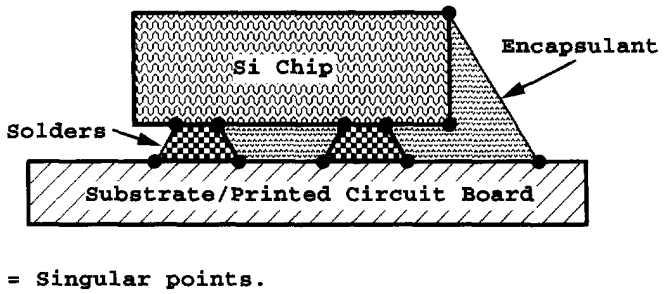

Fig. 1. Typical sites of singular points in an electronic device.

† Research performed while the author served as a visiting assistant professor at the Center for Computational Mechanics, Washington University, Campus Box 1129, St Louis, MO 63130, U.S.A.

$$\mathbf{u}_{EX} = \sum_{i=1}^{\infty} \sum_{m=0}^{M} C_{im} r^{\alpha_i} \ln^m r \mathbf{f}_{im}(\theta) \tag{1}$$

where r, θ are the coordinates of a cylindrical coordinate system located in the singular point and C_{im} are the coefficients of the asymptotic expansion (called the generalized stress intensity factors—GSIFs). The eigenvalues α_i and the eigenfunctions $\mathbf{f}_{im}(\theta)$ are associated pairs (eigenpairs) which depend on the material properties, the geometry, and the boundary conditions in the vicinity of the singular point only. The conditions for power-logarithmic stress singularity to appear ($M \neq 0$) are discussed in Dempsey (1995). Similarly, the solution for problems in linear steady state heat-transfer, in the neighborhood of singular points is as (1), only that the equation is in a scalar form and the coefficients are called generalized flux intensity factors—GFIFs. For general singular points the exact solution $\mathbf{u}_{EX}$ is generally not known explicitly, i.e., neither the exact eigenpairs nor the exact GFIFs/GSIFs are known, therefore a numerical approximation is usually sought. The validity and efficiency of any such numerical method is measured according to the following criteria:

(i) How fast does the numerical approximation converge to the exact value as the number of degrees of freedom (DOF) is increased?
(ii) The robustness of the method. Does the method perform satisfactorily for a large set of very different singular points and input data?

This paper addresses two main topics: first, we propose a set of benchmark test problems for which exact (analytic) solutions are known. The problems have been designed to be representative of the types of singularities present in practical engineering problems associated with linear steady state heat transfer and elastostatic models, and are described in detail to allow their reproduction. Singular points which give rise to complex eigenpairs, as well as logarithmic type singularities ($M \neq 0$ in (1)) are presented. The intended purpose of the proposed problems is to help users and developers of numerical methods to ascertain the accuracy and robustness of the numerical codes used. Thermoelastic problems and cases where non-homogeneous terms are involved (i.e., body forces and non-zero temperature/displacement or flux/traction in the vicinity of the singularities) are not discussed.

In the second part of the paper, the test problems are solved by new numerical methods formulated in detail and analyzed mathematically in (Yosibash 1994, Yosibash and Szabó 1995b and Szabó and Yosibash 1996). Herein, only a short description of the methods, limited to the most essential features, is provided. These methods are used for computing the eigenpairs and the GFIFs/GSIFs numerically, thus demonstrating the efficiency, accuracy and robustness which can be achieved for different types of singularities. Importantly, the numerical algorithm is general in the sense that it first computes the eigenpairs associated with the singular point, which are subsequently used to extract the GFIFs/GSIFs from a p-version finite element solution. New results on the performance of the numerical algorithms applied to problems at multi-material internal interfaces, fixed-free corners and cases involving power-logarithmic stress singularities are reported herein for the first time.

The outline of this paper is as follows. A brief background on related work is given in the following. Sections 2 and 3 contain the set of benchmark test problems associated with steady-state heat transfer and elastostatic models. The numerical methods, based on the p-version of the finite element method, are briefly presented in Section 4 for the heat-transfer problem only, limited to the most essential features. The results obtained are listed and discussed in Section 5 and the conclusions summarized in Section 6. An example problem in linear elasticity where power-logarithmic stress singularities are excited is provided in Appendix A.

1.1. *Related work*

Most of the research performed in the past concentrated on problems corresponding to isotropic materials. In this case, the eigenpairs can be computed analytically (Williams, 1952). For example, in Rice and Sih (1965) the eigenpairs for cracks along the interface

of two dissimilar isotropic materials are explicitly given, and in Suo (1989) explicit eigenfunctions for a crack along the interface of anisotropic materials are provided as well. It is easier to obtain explicit eigenvalues than eigenfunctions (see, for example, Ying (1986) and Dempsey and Sinclair (1981) for cases of up to three sub-domains). For traction-free crack tip singularities the first two coefficients of the asymptotic expansion, usually called the stress intensity factors, can be computed analytically for simple geometries and loading conditions (Murakami, 1987), or can be approximated numerically, usually by the finite element method. See Whiteman and Akin (1979) and Atluri and Nakagaki (1986) for surveys of the main ideas. Finite element methods based on the displacement formulation (principle of minimum potential energy) used to compute the stress intensity factors in isotropic materials can be found, for example, in Szabó and Babuška (1988), Yosibash and Schiff (1993), and Banks-Sills and Sherman (1986). For numerical methods used to compute the stress intensity factors associated with cracks in dissimilar materials we refer to Lin and Mar (1976), Hong and Stern (1978) and Matos *et al.* (1989). Analytical methods for the computation of eigenvalues associated with interface cracks in anisotropic composites can be found in Ting (1986) and the references therein. These methods provide an understanding on the nature of the eigenvalues, but they are complicated for general applications.

Most of the numerical methods, however, are applicable to flux-free crack tip singularities in isotropic materials, do not provide any desired number of stress intensity factors, and fail when the eigenpairs are complex. They are difficult or even impossible to incorporate into standard finite element programs, and moreover, are restricted to a particular type of singularity.

2. HEAT-TRANSFER PROBLEMS

Steady state linear heat-transfer problems (also called scalar problems) in the neighborhood of singular points are considered in this section. Here u denotes the temperature field in a domain. The governing equation is:

$$\sum_{i,j=1}^{2} a_{ij} \frac{\partial^2 u}{\partial x_i \partial x_j} = 0, \tag{2}$$

where a_{ij} are constant coefficients in each sub-domain called coefficients of heat conduction. $a_{ij} = a_{ji}$ and a_{ij} satisfy the elliptic restriction, i.e., $a_{11}a_{22} - a_{12}^2 > 0$ in each sub-domain. For multi-material interfaces we assume that the materials are perfectly bonded together, i.e.,:

$$\begin{aligned} u(r, \theta_k - 0) &= u(r, \theta_k + 0) \\ (a_{ij}^{(k)} v_i \partial_i u)(r, \theta_k - 0) &= (a_{ij}^{(k+1)} v_i \partial_i u)(r, \theta_k + 0) \end{aligned} \tag{3}$$

where $\partial_i u$ symbolizes $\partial u / \partial x_i$, $\mathbf{v} \equiv (v_1, v_2)$ is the unit outward normal vector to the straight line interface between materials k and $k+1$, and $a_{ij}^{(k)}$ are coefficients of heat conduction in each sub-domain. We define the "energy" in a domain Ω by:

$$\mathscr{E}(u) \stackrel{\text{def}}{=} \int\int_{\Omega} \left| a_{11} \left(\frac{\partial u}{\partial x_1} \right)^2 + 2a_{12} \frac{\partial u}{\partial x_1} \frac{\partial u}{\partial x_2} + a_{22} \left(\frac{\partial u}{\partial x_2} \right)^2 \right| \mathrm{d}\Omega,$$

and the energy norm by:

$$\|u\|_E \stackrel{\text{def}}{=} \sqrt{\mathscr{E}(u)}.$$

If a numerical method is used to compute u_{EX}, it can be shown that the relative error between u_{NUM} and u_{EX}, measured in the energy norm can be computed by (Szabó and Babuška (1991) chapter 4):

$$\|e_r\|_E \overset{\text{def}}{=} \frac{\|u_{NUM}-u_{EX}\|_E}{|u_{EX}\|_E} = \sqrt{\frac{|\mathscr{E}(u_{NUM})-\mathscr{E}(u_{EX})|}{|\mathscr{E}(u_{EX})|}}.$$

$\|e_r\|_E$ is a natural measure of convergence of the global numerical solution to the exact solution, frequently used in finite element computations. We will use this measure in the sequel, omitting the subscript r.

2.1. *Scalar problem* 1 : *isotropic clamped-free crack*

Let Ω be the unit circle slit along the positive x axis, and denote by Γ_1 the upper face of the slit, by Γ_2 the lower face of the slit, and by Γ_R the circular portion of the boundary of Ω. (See Fig. 2.) Consider the problem discussed in Babuška and Miller (1984):

$$\nabla^2 u = 0 \quad \text{in } \Omega,$$
$$u = 0 \quad \text{on } \Gamma_1, \quad \frac{\partial u}{\partial \theta} = 0 \quad \text{on } \Gamma_2, \quad \frac{\partial u}{\partial r} = y \quad \text{on } \Gamma_R. \tag{4}$$

Then the solution to this problem, accurate up to the sixth significant digit, is given by Babuška and Miller (1984):

$$u(r,\theta) = -1.35812 r^{1/4}\sin(\theta/4) + 0.970087 r^{3/4}\sin(3\theta/4) + 0.452707 r^{5/4}\sin(5\theta/4) + O(r^{7/4}). \tag{5}$$

and the exact "energy" is $\mathscr{E}(u) = 4.52707$.

2.2. *Scalar problem* 2 : *anisotropic domain*

Consider the heat transfer problem in an anisotropic material governed by the equation:

$$a_{11}\frac{\partial^2 u}{\partial x_1^2} + a_{22}\frac{\partial^2 u}{\partial x_2^2} = 0, \quad a_{11} = 4, \quad a_{22} = 1, \tag{6}$$

prescribed over a domain Ω whose boundary consists of a reentrant corner of 90° generated by two edges, Γ_1 and Γ_2. On the two edges Γ_1 and Γ_2, which meet at the origin of the coordinate system, flux free boundary conditions are applied:

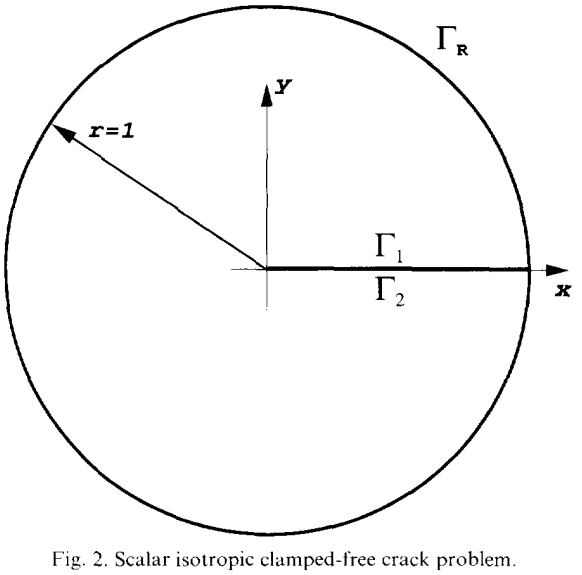

Fig. 2. Scalar isotropic clamped-free crack problem.

$$\sum_{i,j=1}^{2} a_{ij} \frac{\partial u}{\partial x_i} v_j = 0 \quad \text{on } \Gamma_1, \Gamma_2, \tag{7}$$

and $u = 0$ is specified at $(0, 0)$. The solution u can be written in the following form:

$$u = \sum_{n=1}^{\infty} A_n r^{2n/3} 2^{-2n/3} (1 + 3\sin^2\theta)^{n/3} \cos\left[\frac{2n}{3} \arctan(2\tan\theta)\right], \tag{8}$$

where r and θ are polar coordinates centered on the reentrant corner such that $\theta = 0$ coincides with the Γ_1 boundary. The first term in the expansion (8) for ∇u is unbounded as $r \to 0$.

Let Ω be the unit circle sector shown in Fig. 3. The circular boundary of the domain, Γ_R, is loaded by flux boundary condition which corresponds to the first symmetric eigenfunction of the asymptotic expansion of u about the reentrant corner:

$$\begin{aligned} \frac{\partial u}{\partial r} \overset{\text{def}}{\equiv} q_r &= (a_{11}\cos^2\theta + a_{22}\sin^2\theta)\frac{\partial u}{\partial r} + \tfrac{1}{2}\sin 2\theta (a_{22} - a_{11})\left(\frac{1}{r}\frac{\partial u}{\partial \theta}\right) \\ &= A_1 r^{-1/3}[2(1 + 3\sin^2\theta)]^{-2/3}\{\tfrac{2}{3}[(1 + 3\cos^2\theta)(1 + 3\sin^2\theta) - \tfrac{3}{2}\sin^2 2\theta] \\ &\quad \cdot \cos[\tfrac{2}{3}\arctan(2\tan\theta)] + 2\sin 2\theta \sin[\tfrac{2}{3}\arctan(2\tan\theta)]\}. \end{aligned} \tag{9}$$

On the other two boundaries flux-free boundary conditions are applied. The GF1F A_1 is arbitrarily selected to be $A_1 = 1$, while the others are $A_i = 0$, $i = 2, 3, \ldots \infty$. The exact solution to this problem is given by $u_{EX} = u^{(1)}(r, \theta)$.

2.3. *Scalar problem* 3: *internal interface with two materials*

Two-dimensional bodies consisting of two or more materials perfectly bonded along all their common edges attracted scant attention in the past. Lately, with the growing interest in electronic packaging, more attention is focused on the solution to these problems.

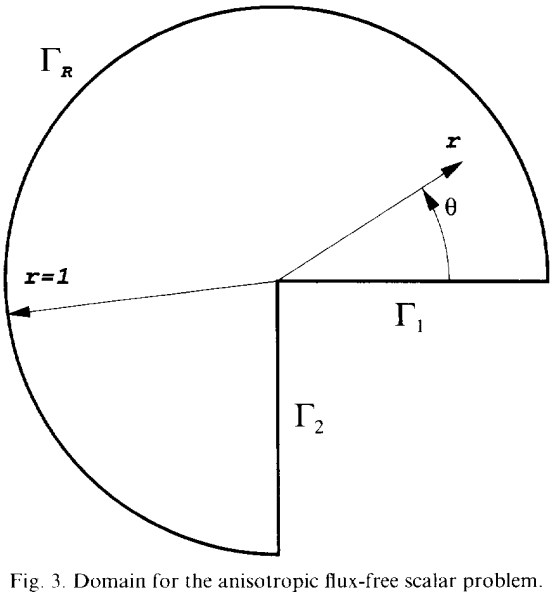

Fig. 3. Domain for the anisotropic flux-free scalar problem.

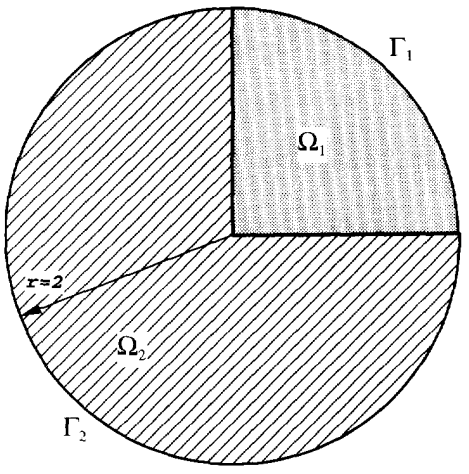

Fig. 4. Internal interface with two materials.

Let $\Omega = \{(r,\theta): r \leqslant 2,\ 0 \leqslant \theta \leqslant 2\pi\}$ and let Ω_i be the two sub-domains of Ω occupying the sectors $0 \leqslant \theta \leqslant \pi/2$, and $\pi/2 \leqslant \theta \leqslant 2\pi$. (See Fig. 4.)

Consider the following interface problem:

$$p_i \nabla^2 u = 0 \quad \text{in}\,\Omega_i, \tag{10}$$

with the following boundary conditions:

$$\frac{\partial u}{\partial r} = p_i[\lambda_1 r^{\lambda_1 - 1} h_1(\theta) + \lambda_2 r^{\lambda_2 - 1} h_2(\theta)] \quad \text{on}\,\Gamma_i = \partial\Omega_i,\ i = 1,2. \tag{11}$$

$$p_1 = 10 \quad \text{and} \quad p_2 = 1$$
$$\lambda_1 = 0.731691779 \quad \text{and} \quad \lambda_2 = 1.268308221 \tag{12}$$

and

$$h_1(\theta) = \begin{cases} \cos[(1-a)\theta] + c_1 \sin[(1-a)\theta] & 0 \leqslant \theta \leqslant \pi/2, \\ c_1 \cos[(1-a)\theta] + c_2 c_3 \sin[(1-a)\theta] & \pi/2 \leqslant \theta \leqslant 2\pi, \end{cases} \tag{13}$$

$$h_2(\theta) = \begin{cases} \cos[(1+a)\theta] - c_3 \sin[(1+a)\theta] & 0 \leqslant \theta \leqslant \pi/2, \\ c_1 \cos[(1+a)\theta] - c_2 c_3 \sin[(1+a)\theta] & \pi/2 \leqslant \theta \leqslant 2\pi, \end{cases} \tag{14}$$

$c_1 = 6.31818181818182$, $c_2 = -2.68181818181818$, $c_3 = 0.64757612580273$ and $a = 0.26830822130025$.

Then the unique solution (up to an additive constant) to this interface problem is given by Oh and Babuška (1992):

$$u(r,\theta) = A_1 r^{\lambda_1} h_1(\theta) + A_2 r^{\lambda_2} h_2(\theta), \tag{15}$$

where $A_1 = A_2 = 1$.

3. ELASTOSTATIC PROBLEMS

Linear elastostatic problems in the neighborhood of singular points are considered in this section. Here $\mathbf{u} \stackrel{\text{def}}{=} (u_x, u_y)^T$ denotes the displacement vector in the x, y directions and σ_x, σ_y, τ_{xy} are the stresses. For multi-material interfaces we assume continuity of dis-

placements and tractions across boundary interfaces. We define the "strain energy" in a domain Ω by:

$$\mathscr{E}(\mathbf{u}) \stackrel{\text{def}}{=} \frac{1}{2}\int\int_{\Omega} ([\mathbf{D}]\mathbf{u})^{\mathrm{T}}[\mathbf{E}][\mathbf{D}]\mathbf{u}\,\mathrm{d}\Omega,$$

where $[\mathbf{E}]$ is the 3×3 material matrix, and

$$[\mathbf{D}] \stackrel{\text{def}}{=} \begin{bmatrix} \partial/\partial x & 0 \\ 0 & \partial/\partial y \\ \partial/\partial y & \partial/\partial x \end{bmatrix}.$$

The energy norm and its connection to the strain energy is equivalent to that presented in the previous section, i.e.

$$\|\mathbf{u}\|_E \stackrel{\text{def}}{=} \sqrt{\mathscr{E}(\mathbf{u})}.$$

3.1. *Elastostatic problem* 1 : *traction-free isotropic L-shaped domain*

Let us consider the L-shaped plane elastic body presented in Fig. 5, having re-entrant edges of length 1. On the boundaries of the domain, tractions which correspond to the following exact stress field:

$$\begin{aligned}
\sigma_x &= A_1\alpha_1 r^{\alpha_1-1}\{[2-Q_1(\alpha_1+1)]\cos(\alpha_1-1)\theta-(\alpha_1-1)\cos(\alpha_1-3)\theta\} \\
&\quad + A_2\alpha_2 r^{\alpha_2-1}\{[2-Q_2(\alpha_2+1)]\sin(\alpha_2-1)\theta-(\alpha_2-1)\sin(\alpha_2-3)\theta\} \\
\sigma_y &= A_1\alpha_1 r^{\alpha_1-1}\{[2+Q_1(\alpha_1+1)]\cos(\alpha_1-1)\theta+(\alpha_1-1)\cos(\alpha_1-3)\theta\} \\
&\quad + A_2\alpha_2 r^{\alpha_2-1}\{[2+Q_2(\alpha_2+1)]\sin(\alpha_2-1)\theta+(\alpha_2-1)\sin(\alpha_2-3)\theta\} \\
\tau_{xy} &= A_1\alpha_1 r^{\alpha_1-1}\{(\alpha_1-1)\sin(\alpha_1-3)\theta+Q_1(\alpha_1+1)\sin(\alpha_1-1)\theta\} \\
&\quad + A_2\alpha_2 r^{\alpha_2-1}\{(\alpha_2-1)\cos(\alpha_2-3)\theta+Q_2(\alpha_2+1)\cos(\alpha_2-1)\theta\}
\end{aligned} \tag{16}$$

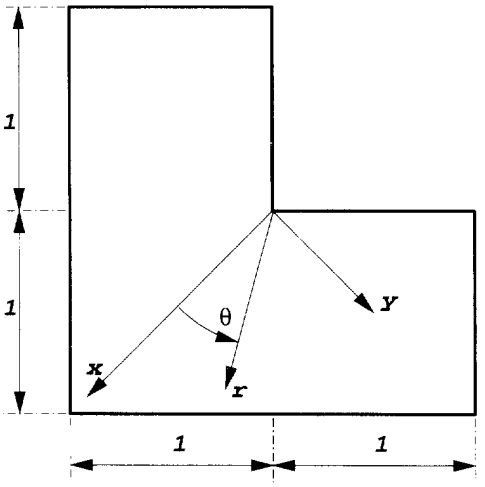

Fig. 5. The L-shaped domain.

are being applied where A_1 and A_2 are constants analogous to the mode 1 and 2 stress intensity factors in linear elastic fracture mechanics; $\alpha_1 = 0.5444837368$, $Q_1 = 0.543075597$, $\alpha_2 = 0.9085291898$, $Q_2 = -0.218923236$ are constants determined so that the solution satisfies the equilibrium equations and the traction-free boundary conditions on the re-entrant edges.

3.2. *Elastostatic problem* 2: *traction-fee crack in an isotropic material*

Let us consider the plane elastic body with a crack along the negative x-axis shown in Fig. 6, which is isotropic with material constants $E = 1$ and $\nu = 0.3$, presented in Szabó and Babuška (1988). On the boundaries of the domain, tractions which correspond to the exact stress field given by (16) are being applied where A_1 and A_2 are the mode 1 and 2 stress intensity factors in linear elastic fracture mechanics; $\alpha_1 = \alpha_2 = 1/2$, $Q_1 = 1/3$ and $Q_2 = -1$ are constants determined so that the solution satisfies the equilibrium equations and the traction-free boundary conditions on the re-entrant edges. Furthermore, the displacement vector at $(0,0)$ is fixed and the y-components of the displacement vector at $(1,0)$ is fixed.

3.3. *Elastostatic problem* 3: *fixed-free* 90° *isotropic corner*

Plane problems (or axisymmetric problems) with rigidly fixed end and traction free lateral surface are of increasingly interest in contact mechanics, for example, when an elastic body is compressed between rough rigid stamps, with the contact being without slip. A representative case for these problems, where the stresses are singular, for which an analytic solution is available is presented in Fig. 7. The origin of a polar coordinate system is placed at the corner with $\theta = 0$ being the fixed edge:

$$\begin{cases} u_x(\theta = 0) = 0 \\ u_y(\theta = 0) = 0 \end{cases} \tag{17}$$

and a traction free edge is assumed at $\theta = \pi/2$:

$$\begin{cases} T_x(\theta = \pi/2) = 0 \\ T_y(\theta = \pi/2) = 0 \end{cases} \tag{18}$$

Consider a plane-strain situation for which $\kappa = 3 - 4\nu$, and material properties $E = 1$ and

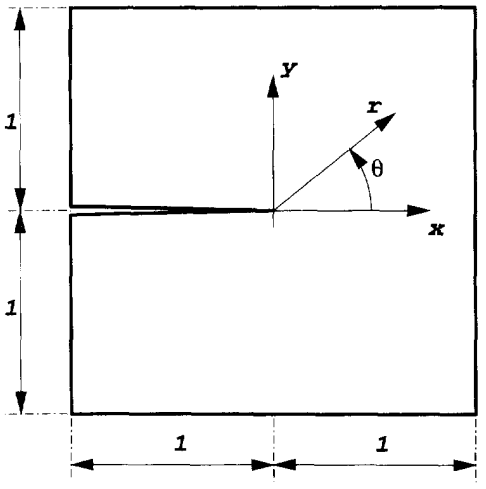

Fig. 6. Crack in an isotropic domain.

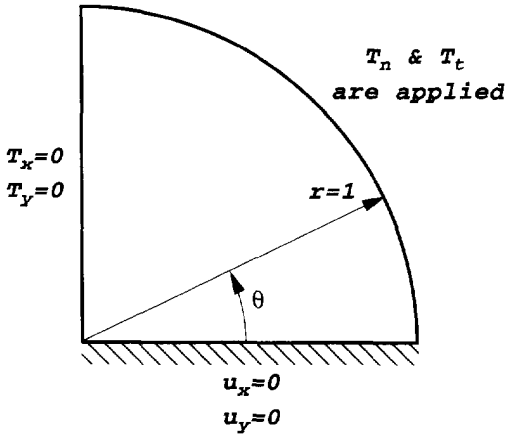

Fig. 7. Fixed-free 90° isotropic corner.

$v = 0.3$. The exact value of the strength of the singularity α_i, at $r \to 0$, can be obtained by solving the implicit equation:

$$\cos(\alpha_i \pi) = \frac{2\alpha_i^2}{\kappa} - \frac{\kappa^2 + 1}{2\kappa}. \tag{19}$$

The first eigenvalue is real $\alpha_1 \overset{\text{def}}{=} \alpha = 0.71117293327$.

Imposing the following traction field on the boundary $r = 1, 0 \geqslant \theta \geqslant \pi/2$:

$$\begin{aligned} T_n(\theta) &= A_1/2.8\{[(3-\alpha)\cos(1-\alpha)\theta - (1.8-\alpha)\cos(1+\alpha)\theta] \\ &\quad -\gamma[(3-\alpha)\sin(1-\alpha)\theta - (1.8+\alpha)\sin(1+\alpha)\theta]\}, \\ T_t(\theta) &= A_1/2.8\{[(1-\alpha)\sin(1-\alpha)\theta + (1.8-\alpha)\sin(1+\alpha)\theta] \\ &\quad +\gamma[(1-\alpha)\cos(1-\alpha)\theta + (1.8+\alpha)\cos(1+\alpha)\theta]\}, \end{aligned} \tag{20}$$

where

$$\gamma = \frac{\sin(\alpha\pi)}{\kappa + 2\alpha + \cos(\alpha\pi)} = 0.302275728, \tag{21}$$

one obtains the exact stress field in the domain, see Stern and Soni (1976):

$$\begin{aligned} \sigma_{rr} &= A_1 r^{(\alpha-1)}/2.8\{[(3-\alpha)\cos(1-\alpha)\theta - (1.8-\alpha)\cos(1+\alpha)\theta] \\ &\quad -\gamma[(3-\alpha)\sin(1-\alpha)\theta - (1.8+\alpha)\sin(1+\alpha)\theta]\}, \\ \sigma_{\theta\theta} &= A_1 r^{(\alpha-1)}/2.8\{[(1+\alpha)\cos(1-\alpha)\theta + (1.8-\alpha)\cos(1+\alpha)\theta] \\ &\quad -\gamma[(1+\alpha)\sin(1-\alpha)\theta + (1.8+\alpha)\sin(1+\alpha)\theta]\}, \\ \sigma_{r\theta} &= A_1 r^{(\alpha-1)}/2.8\{[(1-\alpha)\sin(1-\alpha)\theta + (1.8-\alpha)\sin(1+\alpha)\theta] \\ &\quad +\gamma[(1-\alpha)\cos(1-\alpha)\theta + (1.8+\alpha)\cos(1+\alpha)\theta]\}. \end{aligned} \tag{22}$$

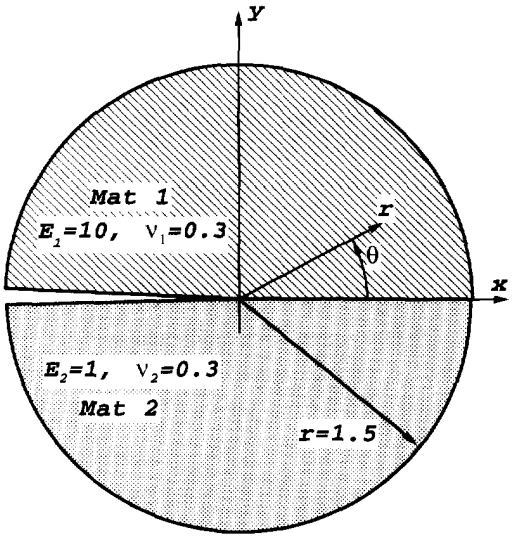

Fig. 8. Crack at a bi-material interface example problem.

3.4. *Elastostatic problem* 4: *traction-free crack at isotropic bi-material interface*

A bi-material is a composite of two homogeneous materials, with continuity of tractions and displacements across interfaces maintained. For two isotropic materials, an exact solution for the stress tensor can be obtained using complex analysis. Consider a domain presented in Fig. 8, and define:

$$\varepsilon = \frac{1}{2\pi} \ln \left(\frac{\kappa_1 \mu_2 + \mu_1}{\kappa_2 \mu_1 + \mu_2} \right) \tag{23}$$

where

$$\kappa = \begin{cases} 3 - 4\nu & \text{for plane strain} \\ (3-\nu)/(1+\nu) & \text{for plane stress} \end{cases}$$

and μ is the shear modulus. This domain is loaded by normal and tangential tractions on the circular boundary as follows:

$$T_n(r = 1.5, \theta) = \frac{1}{\sqrt{3\pi}} \{ K_I [\cos(\varepsilon \ln 1.5)\sigma_{rr}^{\mathfrak{R}} + \sin(\varepsilon \ln 1.5)\sigma_{rr}^{\mathfrak{I}}] + K_{II}[-\sin(\varepsilon \ln 1.5)\sigma_{rr}^{\mathfrak{R}} + \cos(\varepsilon \ln 1.5)\sigma_{rr}^{\mathfrak{I}}] \} \tag{24}$$

$$T_t(r = 1.5, \theta) = \frac{1}{\sqrt{3\pi}} \{ K_I [\cos(\varepsilon \ln 1.5)\sigma_{r\theta}^{\mathfrak{R}} + \sin(\varepsilon \ln 1.5)\sigma_{r\theta}^{\mathfrak{I}}] + K_{II}[-\sin(\varepsilon \ln 1.5)\sigma_{r\theta}^{\mathfrak{R}} + \cos(\varepsilon \ln 1.5)\sigma_{r\theta}^{\mathfrak{I}}] \}, \tag{25}$$

where σ_{rr} and $\sigma_{r\theta}$ are given by (27), and K_I, K_{II} are the so-called "stress intensity factors" in fracture mechanics. The crack faces are traction-free.

Following Suo (1989)†, the exact stress fields in material 1 can be put into the form:

† The expressions for the displacements in Suo (1989) are not continuous across the interface at $\theta = 0$, therefore could not possibly be valid.

$$\sigma_{ij} = \frac{1}{\sqrt{2\pi r}}\{K_I[\cos(\varepsilon \ln r)\sigma_{ij}^{\mathscr{R}} + \sin(\varepsilon \ln r)\sigma_{ij}^{\mathscr{I}}] + K_{II}[-\sin(\varepsilon \ln r)\sigma_{ij}^{\mathscr{R}} + \cos(\varepsilon \ln r)\sigma_{ij}^{\mathscr{I}}]\} \quad i,j = r,\theta, \tag{26}$$

where

$$\begin{aligned}
\sigma_{rr}^{\mathscr{R}} &= [-\sinh \varepsilon(\pi-\theta)\cos(3\theta/2) + e^{-\varepsilon(\pi-\theta)}\cos(\theta/2)(1+\sin^2(\theta/2)+\varepsilon\sin(\theta))]/c \\
\sigma_{\theta\theta}^{\mathscr{R}} &= [\sinh \varepsilon(\pi-\theta)\cos(3\theta/2) + e^{\varepsilon(\pi-\theta)}\cos(\theta/2)(\cos^2(\theta/2)-\varepsilon\sin(\theta))]/c \\
\sigma_{r\theta}^{\mathscr{R}} &= [\sinh \varepsilon(\pi-\theta)\sin(3\theta/2) + e^{-\varepsilon(\pi-\theta)}\sin(\theta/2)(\cos^2(\theta/2)-\varepsilon\sin(\theta))]/c \\
\sigma_{rr}^{\mathscr{I}} &= [\cosh \varepsilon(\pi-\theta)\sin(3\theta/2) - e^{-\varepsilon(\pi-\theta)}\sin(\theta/2)(1+\cos^2(\theta/2)-\varepsilon\sin(\theta))]/c \\
\sigma_{\theta\theta}^{\mathscr{I}} &= [-\cosh \varepsilon(\pi-\theta)\sin(3\theta/2) - e^{-\varepsilon(\pi-\theta)}\sin(\theta/2)(\sin^2(\theta/2)+\varepsilon\sin\theta))]/c \\
\sigma_{r\theta}^{\mathscr{I}} &= [\cosh \varepsilon(\pi-\theta)\cos(3\theta/2) + e^{-\varepsilon(\pi-\theta)}\cos(\theta/2)(\sin^2(\theta/2)+\varepsilon\sin(\theta))]/c \\
c &= \cosh \varepsilon\pi.
\end{aligned} \tag{27}$$

The stress fields in material 2 can be obtained by replacing π by $-\pi$ everywhere in (27). The first singular exponent (first eigenvalue) for this crack problem is a complex number given by $1/2 \pm i\varepsilon$.

3.5. *Elastostatic problem 5: inclusion problem*

The case of a composite body consisting of two dissimilar isotropic, homogeneous and elastic wedges, perfectly bonded along their interfaces, is studied. The analytic (exact) asymptotic series representing the stress field in the neighborhood of the singular point can be derived explicitly for this problem, as shown by Chen (1994).

Consider the unit circle domain Ω, divided into two sectors: Ω_1 occupying the sector $-5\pi/6 \leqslant \theta \leqslant 5\pi/6$ and Ω_2 occupying the sector $5\pi/6 \leqslant \theta \leqslant 7\pi/6$, see Fig. 9. Plane strain condition is assumed with $\nu_1 = \nu_2 = 0.3$ and $E_1 = 10{,}000$, $E_2 = 1$. The eigenvalues characterizing the stress singularity in the vicinity of the point $(x, y) = (0, 0)$ for the modes I and II are given by $\alpha_1 = 0.512472160$ and $\alpha_2 = 0.730975740$. On the boundary of the domain the following traction field is applied:

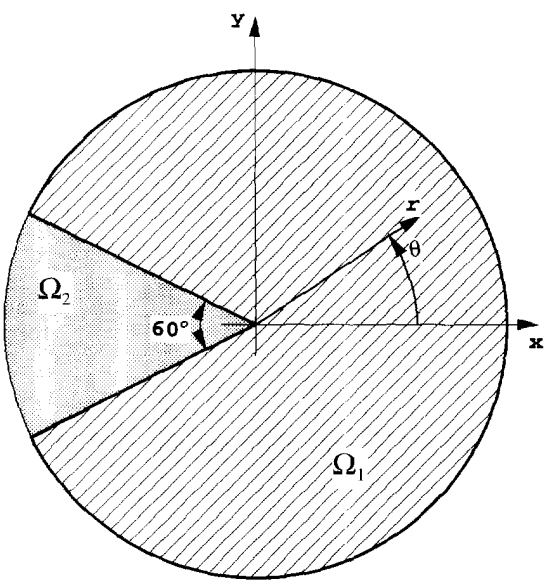

Fig. 9. Domain configuration of the elasticity inclusion problem.

$-5\pi/6 \leqslant \theta \leqslant 5\pi/6$

$$T_n(\theta) = -0.717604531\frac{K_I}{\sqrt{2\pi}}\{0.401735588\cos[(1+\alpha_1)\theta] - 1.561125474\cos[(\alpha_1-1)\theta]\} - 1.023570729\frac{K_{II}}{\sqrt{2\pi}}\{-0.813197463\sin[(1+\alpha_2)\theta] - 1.619121416\sin[(\alpha_2-1)\theta]\} \tag{28}$$

$$T_t(\theta) = 0.717604531\frac{K_I}{\sqrt{2\pi}}\{0.401735588\sin[(1+\alpha_1)\theta] - 0.305963261\sin[(\alpha_1-1)\theta]\} - 1.023570729\frac{K_{II}}{\sqrt{2\pi}}\{-0.813197463\cos[(1+\alpha_2)\theta] - 0.813974463\cos[(\alpha_2-1)\theta]\} \tag{29}$$

$5\pi/6 \leqslant \theta \leqslant 7\pi/6$

$$T_n(\theta) = -0.000370516\frac{K_I}{\sqrt{2\pi}}\{0.972611382\cos[(1+\alpha_1)(\pi-\theta)] - 1.561125474\cos[(\alpha_1-1)(\pi-\theta)]\} + 0.000152306\frac{K_{II}}{\sqrt{2\pi}}\{-1.240586478\sin[(1+\alpha_2)(\pi-\theta)] - 1.619121416\sin[(\alpha_2-1)(\pi-\theta)]\} \tag{30}$$

$$T_t(\theta) = -0.000370516\frac{K_I}{\sqrt{2\pi}}\{0.972611382\sin[(1+\alpha_1)(\pi-\theta)] - 0.305963261\sin[(\alpha_1-1)(\pi-\theta)]\} - 0.000152306\frac{K_{II}}{\sqrt{2\pi}}\{-1.240586478\cos[(1+\alpha_2)(\pi-\theta)] - 0.191969274\cos[(\alpha_2-1)(\pi-\theta)]\}, \tag{31}$$

where K_I and K_{II} are chosen arbitrarily to be $\sqrt{2\pi}$. The exact stress field in the domain is singular at $r = 0$, and can be written in the form:

$$\sigma_{ij}^{EX} = r^{\alpha_1-1}f_{ij}^{(I)}(\theta) + r^{\alpha_2-1}f_{ij}^{(II)}(\theta) \quad ij = r, \theta, r\theta, \tag{32}$$

where $f_{ij}^{I}(\theta)$ and $f_{ij}^{II}(\theta)$ are the functions given by:

$-5\pi/6 \leqslant \theta \leqslant 5\pi/6$

$$f_r^{(I)}(\theta) = -0.717604531\{0.401735588\cos[(1+\alpha_1)\theta] - 1.561125474\cos[(\alpha_1-1)\theta]\}$$

$$f_r^{(II)}(\theta) = -1.023570729\{-0.813197463\sin[(1+\alpha_2)\theta] - 1.619121416\sin[(\alpha_2-1)\theta]\}$$

$$f_\theta^{(I)}(\theta) = 0.717604531\{0.401735588\cos[(1+\alpha_1)\theta] + 0.949198951\cos[(\alpha_1-1)\theta]\}$$

$$f_\theta^{(II)}(\theta) = 1.023570729\{-0.813197463\sin[(1+\alpha_2)\theta] + 1.235182867\sin[(\alpha_2-1)\theta]\}$$

$$f_{r\theta}^{(I)}(\theta) = 0.717604531\,\{0.401735588\sin[(1+\alpha_1)\theta] - 0.305963261\sin[(\alpha_1-1)\theta]\}$$

$$f_{r\theta}^{(II)}(\theta) = -1.023570729\,\{-0.813197463\cos[(1+\alpha_2)\theta] - 0.81397463\cos[(\alpha_2-1)\theta]\}$$

$5\pi/6 \leqslant \theta \leqslant 7\pi/6$

$$\begin{aligned}
f_r^{(I)}(\theta) &= -0.000370516\,\{0.972611382\cos[(1+\alpha_1)(\pi-\theta)] \\
&\quad -1.561125474\cos[(\alpha_1-1)(\pi-\theta)]\} \\
f_r^{(II)}(\theta) &= 0.000152306\,\{-1.240586478\sin[(1+\alpha_2)(\pi-\theta)] \\
&\quad -1.619121416\sin[(\alpha_2-1)(\pi-\theta)]\} \\
f_\theta^{(I)}(\theta) &= 0.000370516\,\{0.972611382\cos[(1+\alpha_1)(\pi-\theta)] \\
&\quad +0.949198951\cos[(\alpha_1-1)(\pi-\theta)]\} \\
f_\theta^{(II)}(\theta) &= -0.000152306\,\{-1.240586478\sin[(1+\alpha_2)(\pi-\theta)] \\
&\quad +1.235182867\sin[(\alpha_2-1)(\pi-\theta)]\} \\
f_{r\theta}^{(I)}(\theta) &= -0.000370516\,\{0.972611382\sin[(1+\alpha_1)(\pi-\theta)] \\
&\quad -0.305963261\sin[(\alpha_1-1)(\pi-\theta)]\} \\
f_{r\theta}^{(II)}(\theta) &= -0.000152306\,\{-1.240586478\cos[(1+\alpha_2)(\pi-\theta)] \\
&\quad -0.191969274\cos[(\alpha_2-1)(\pi-\theta)]\}.
\end{aligned}$$

3.6. *Elastostatic problem* 6: *rigid body motion*

Many numerical formulations do not satisfy the rigid body displacement criteria, meaning that under rigid body translation or rigid body rotations, generating no singularities, the computed GSIFs are not identically zero. To examine this criteria we consider again the plane elastic body with a crack along the negative x-axis shown in Fig. 6. This time we subject the domain to large rigid body translations by imposing on its boundaries rigid body displacements:

$$\mathbf{u} = \begin{Bmatrix} 3.0 \\ -3.0 \end{Bmatrix}, \tag{33}$$

and the rigid body rotation:

$$\mathbf{u} = \begin{Bmatrix} y \\ -x \end{Bmatrix}. \tag{34}$$

The strain energy in this case is identically zero as well as the stress intensity factors.

4. THE COMPUTATIONAL SCHEME

4.1. *Eigenpairs computation by the modified Steklov method*

Let us "zoom in" at the singular point and consider a domain Ω_R^* in its vicinity shown in Fig. 10. r, θ are the coordinates of a cylindrical coordinate system located in the singular point. In Ω_R^* the steady-state heat transfer governing equation is given in (2). To simplify our discussion let us assume flux free boundary conditions on Γ_1 and Γ_2, i.e.:

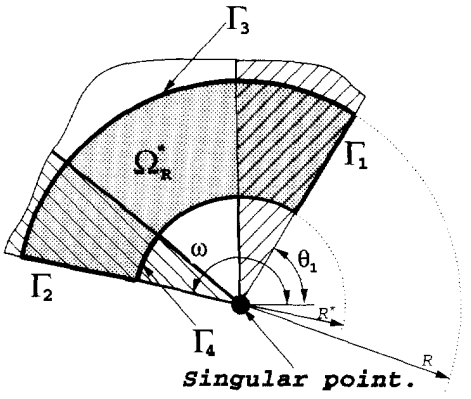

Fig. 10. Domain and notations for modified Steklov formulation.

$$\sum_{i,j=1}^{2} a_{ij} v_j \frac{\partial u}{\partial x_i} = 0 \quad \text{on } \Gamma_1 \text{ and } \Gamma_2. \tag{35}$$

In Ω_R^*, u may be represented as follows: $u = r^x f(\theta)$. Under special (exceptional) circumstances, u may also have additional terms as $r^x \ln(r) f(\theta)$ (see Dempsey (1995)). This case is addressed in Appendix A, and not treated in the following analysis. Therefore, on Γ_1 and Γ_2 we have:

$$(\partial u/\partial r) = (\alpha/R)u. \tag{36}$$

Multiplying (2) by a test function $v \in H^1(\Omega_R^*)$ (H^1 being the usual Sobolev space), integrate using Green's theorem, and following the steps presented in Yosibash (1994), we obtain the following modified Steklov weak form:

Seek $\alpha \in \mathscr{R}$, $0 \neq u \in H^1(\Omega_R^*)$ such that

$$\mathscr{B}(u,v) - (\mathscr{N}_R(u,v) + \mathscr{N}_{R^*}(u,v)) = \alpha(\mathscr{M}_R(u,v) + \mathscr{M}_{R^*}(u,v)), \quad \forall v \in H^1(\Omega_R^*) \tag{37}$$

where:

$$\mathscr{B}(u,v) \overset{\text{def}}{=} \int\int_{\Omega_R^*} \sum_{i,j=1}^{2} a_{ij} \frac{\partial u}{\partial x_i} \frac{\partial v}{\partial x_j} \, d\Omega, \tag{38}$$

$$\mathscr{M}_R(u,v) \overset{\text{def}}{=} \int_{\theta_1}^{\omega} [(a_{11}\cos^2\theta + a_{12}\sin 2\theta + a_{22}\sin^2\theta)uv]_{r=R} \, d\theta, \tag{39}$$

$$\mathscr{N}_R(u,v) \overset{\text{def}}{=} \int_{\theta_1}^{\omega} \left\{ [(a_{22} - a_{11})\sin\theta\cos\theta + a_{12}\cos 2\theta] \frac{\partial u}{\partial \theta} v \right\}_{r=R} d\theta, \tag{40}$$

and similarly for $\mathscr{M}_{R^*}$ and $\mathscr{N}_{R^*}$ only that the integration is performed at $r = R^*$.

Remark 1. The domain Ω_R^* does not include singular points. Also note that the formulation of the weak form has not limited the domain Ω_R^* to be isotropic, and in fact can be applied to multi-material anisotropic interfaces.

Numerical solution by the p-version of the finite element method. The weak eigenproblem (37) is reformulated in the framework of the p-version of the finite element method. The domain Ω_R^* is divided into finite elements through a meshing process. The polynomial basis and trial functions are defined on a standard element in the ξ, η plane such that $-1 < \xi < 1$, $-1 < \eta < 1$. These elements are then mapped by appropriate mapping functions onto the

"real" elements (for details see Szabó and Babuška (1991) chapters 5 and 6). Let u be expressed in terms of the basis functions in the standard plane $\Phi_i(\xi, \eta)$:

$$u(\xi, \eta) = \sum_{i=1}^{N} b_i \Phi_i(\xi, \eta) \tag{41}$$

where b_i are the amplitudes of the basis functions (sometimes called the "nodal values"), and Φ_i are products of integrals of Legendre polynomials in ξ and η. Denoting the set of coefficients associated with Γ_3 and Γ_4 by $\{b_R\}$, we obtain after performing static condensation the following eigenproblem:

$$[\mathbf{K}_s]\{b_R\} = \alpha[\mathbf{M}]\{b_R\}, \tag{42}$$

where $[\mathbf{K}_s]$ is the condensed stiffness matrix associated with the left hand side of (37) and $[\mathbf{M}]$ is the matrix associated with the right hand side of (37). The solution of the eigenproblem (42) provides the sought eigenvalues α_i and the associated eigenvectors. For details the reader is referred to Yosibash (1994) and Yosibash and Szabó (1995b).

4.2. *Extraction of the GFIFs*

Once the eigenpairs are computed, they are used for extracting the GFIFs. The procedure is as follows. First we solve the problem over the entire domain of interest Ω by means of the finite element method based on the displacement formulation, thus obtaining u_{FE}. Second, a small sub-domain around the singular point P is constructed. Define S_R as the interior points of a circle of radius R centered on the point P. Ω_R is defined by $\Omega \cap S_R$ and Γ_R is its circular boundary. (See Fig. 11.) Defining $\mathbf{q}_0 \overset{\text{def}}{=} (\partial u/\partial x,\ \partial u/\partial y)^{\mathrm{T}}$, and $\mathbf{q}_1 \overset{\text{def}}{=} (\partial v/\partial x, \partial v/\partial y)^{\mathrm{T}}$ then the complementary variational principle over Ω_R can be stated as:

$$\text{Seek} \quad \mathbf{q}_0 \in E_c(\Omega_R), \quad \text{such that:}$$

$$\mathscr{B}_c(\mathbf{q}_0, \mathbf{q}_1) \overset{\text{def}}{=} \int_0^R \int_{\theta_1}^{\omega} \sum_{i,j=1}^{2} a_{ij} \frac{\partial u}{\partial x_i} \frac{\partial v}{\partial x_j} r \, \mathrm{d}r \, \mathrm{d}\theta$$

$$= \int_{\Gamma_R} \hat{u} \sum_{i,j=1}^{2} a_{ij} \frac{\partial v}{\partial x_i} v_j \, \mathrm{d}s \overset{\text{def}}{=} \mathscr{F}_c(\mathbf{q}_1) \quad \forall \mathbf{q}_1 \in E_c(\Omega_R), \tag{43}$$

$E_c(\Omega_R)$ being the statically admissible space (see detailed definition in Szabó and Babuška

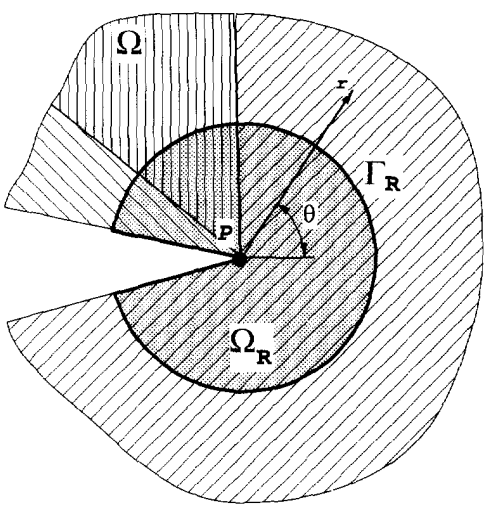

Fig. 11. The domain Ω and the extraction sub-domain Ω_R.

(1991)), and $\hat{u}$ is the temperature along Γ_R. Since $\hat{u}$ in (43) is not known exactly, it is replaced with the approximated finite element solution u_{FE}.

For the complementary weak form the trial and test spaces $\mathbf{q}_0$ and $\mathbf{q}_1$, are chosen to be linear combinations of the eigenfluxes, which are computed from the eigenpairs using temperature-flux relationship. The unknowns are the GFIFs.

Remark 2. The eigen-flux vector, being derived from the eigenpairs, automatically satisfies the boundary conditions on all boundaries except Γ_R, so that the linear form $\mathscr{F}_c(\mathbf{q}_1)$ degenerates to an integral over the circular boundary Γ_R alone.

Solving (43), one obtains an approximation for the series coefficients, the GFIFs. Mathematical analysis (see Yosibash (1994) and Szabó and Yosibash (1996)) followed by numerical examples demonstrate that the rate of convergence of the GFIFs to the exact values is as fast as the convergence of the energy, therefore the method is "super-convergent".

5. NUMERICAL RESULTS AND DISCUSSION

The algorithms presented in Section 4 have been implemented in the p-version finite element computer code PEGASYS† which was used for performing the numerical studies. The trunk space was used to represent the trial and test function space in all computations. By definition, the trunk space of degree p spans the set of monomials $\xi^i\eta^j$, $i+j \leqslant p$ augmented by the monomial $\xi\eta$ for $p = 1$ and by the monomials $\xi^p\eta$, $\xi\eta^p$ for $p \geqslant 2$ on the standard quadrilateral element defined by $\Omega_{st}^q = \{\xi,\eta : |\xi| \leqslant 1, \quad |\eta| \leqslant 1\}$. Elements are mapped by the blending function method. Therefore the boundaries are represented exactly in the stiffness matrix and load vector computations. The load vectors were computed by evaluating the applied tractions in 14 Gauss points along the loaded edge of each element and integrated numerically, using double precision operations. The trial functions over each element are polynomials of degree $1 \leqslant p \leqslant 8$, and the integration scheme uses $(p+3)(p+3)$ Gauss integration points over each quadrilateral.

The performance of the numerical methods presented in Section 4 is reported in the following. The set of benchmark problems is solved, and the computed eigenvalues and GFIFs/GSIFs are presented. As demonstrated in the sequel, the proposed methods provide results of high accuracy, are robust and efficient.

5.1. *Scalar problem* 1 : *results*

This particular example problem was chosen to demonstrate that the proposed method has the same super-convergent properties as the extraction method proposed in Babuška and Miller (1984). The extraction method in Babuška and Miller (1984), however, requires the knowledge of the eigenpairs *a priori*, and is not applicable to anisotropic materials.

This problem has been solved in Yosibash (1994) using the exact known eigenpairs. Herein, the eigenpairs are computed numerically using the modified Steklov method resulting in $(\alpha_1)_{approx} = 0.250000000002$, $(\alpha_2)_{approx} = 0.750000000000$ and $(\alpha_3)_{approx} = 1.250000000000$ at $p = 8$ (CPU time to compute these values was 3.31 s on a Silicon Graphics IRIS Indigo workstation R3000, 24MB of RAM, SpecMark89 = 28). The high accuracy of the computed eigenpairs is essential in computing the GFIFs.

For the extraction of the GFIFs, the mesh shown in Fig. 12 is used with 2 refinement layers toward the singular point, one having the radius of 0.15 and the other having the radius of 0.15^2. The GFIFs are extracted using an integration path $R = 0.9$ with 10 terms in the series. In Table 1 we summarize the approximated first three GFIFs, their relative error $(e_{A_i}(\%) \equiv 100(A_i^{FE} - A_i)/A_i)$, the corresponding number of degrees of freedom and the relative error in energy norm. The following conclusions may be drawn from the results shown in Table 1 which are typical of many other numerical experiments performed:

† PEGASYS is a trademark of Engineering Software Research and Development, Inc. 7750 Clayton Road, Suite 204, St Louis, MO 63117.

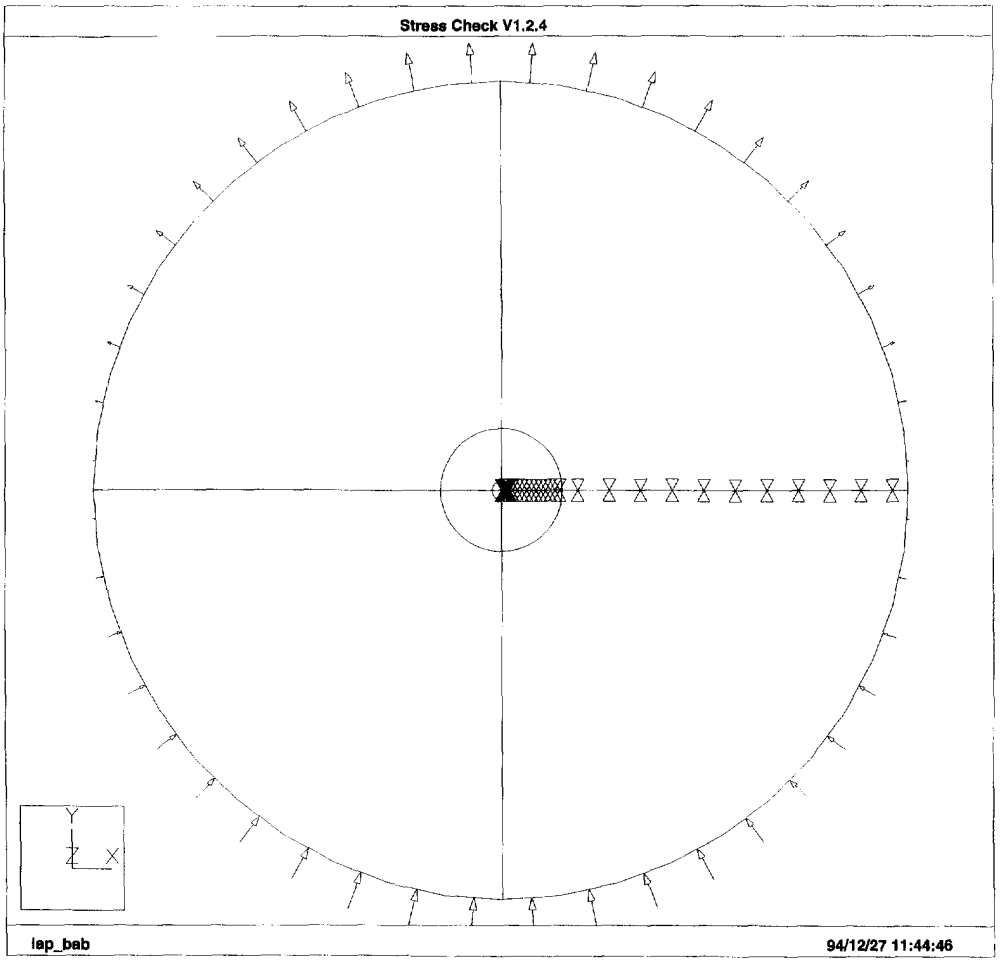

Fig. 12. F. E. mesh and boundary condition for scalar problem 1.

(i) Despite the presence of a strong ($r^{1/4}$-type) singularity, A_1^{FE} appears to be converging at a rate which is at least twice that of the error in energy norm. This rate of convergence is approximately the same as that reported in Babuška and Miller (1984).

(ii) The GFIFs A_2^{FE} and A_3^{FE} are much more accurate than A_1^{FE} (the error is smaller than that reported in Babuška and Miller (1984)), and the observed convergence rate is considerably faster when compared with the convergence of the error in energy norm.

(iii) For path radii taken far enough from the singular point, $R > 0.5$ in this example problem, the accuracy of the GFIFs is almost independent of R.

Table 1. Computed values of the first three GFIFs for scalar problem 1, $R = 0.9$

	$p=1$	$p=2$	$p=3$	$p=4$	$p=5$	$p=6$	$p=7$	$p=8$
DOF	12	36	64	104	156	220	296	384
$\|e\|_E(\%)$	34.52	16.73	12.79	11.26	10.25	9.49	8.89	8.39
A_1^{FE}	−1.106246	−1.261053	−1.286924	−1.313504	−1.313504	−1.319999	−1.324789	−1.328490
$e_{A_1}(\%)$	−18.54	−7.15	−5.24	−3.94	−3.28	−2.81	−2.45	−2.18
A_2^{FE}	0.893839	0.971012	0.969531	0.970206	0.97007	0.970077	0.970090	0.970085
$e_{A_2}(\%)$	−7.86	0.095	−0.057	0.012	<0.0001	−0.0010	0.00031	−0.0002
A_3^{FE}	0.379149	0.446053	0.452521	0.452492	0.452694	0.452706	0.452705	0.452708
$e_{A_3}(\%)$	−16.25	−1.47	−0.0411	−0.0475	−0.0029	−0.0002	−0.0004	0.0002

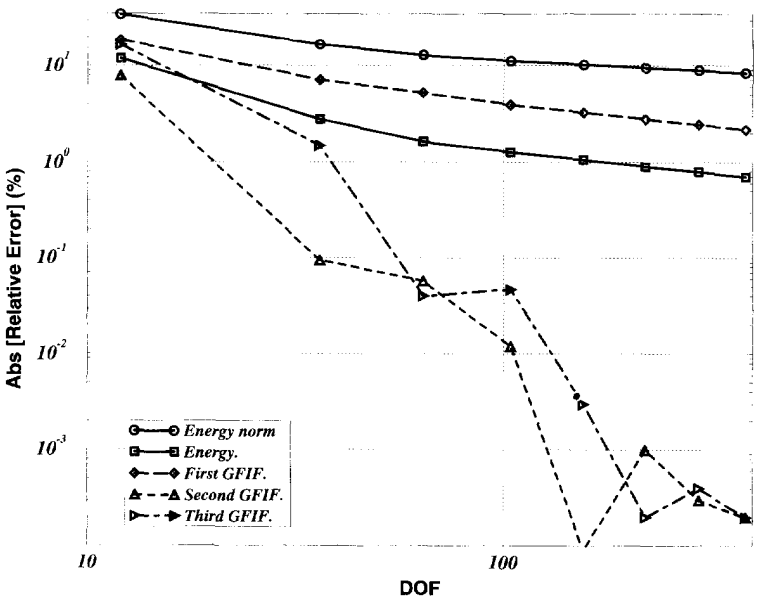

Fig. 13. Convergence of the relative error in energy norm, energy and the first three GFIFs for scalar problem 1.

(iv) As expected, for isotropic materials, the number of terms considered in the series has no influence on the accuracy of the GFIFs.

We present in Fig. 13 the convergence of the GFIFs as compared with the relative error in energy norm and the relative error in energy. Note that the rate of convergence in the first GFIF is faster than the rate of convergence of the energy norm, and at $p > 4$ is virtually the same as the rate of convergence of the energy. The second and third GFIFs converge much faster. This is because the corresponding eigenfunctions are much smoother.

5.2. *Scalar problem* 2: *results*

The eigenpairs were computed using the modified Steklov method, obtaining the first three approximated eigenvalues: $\alpha_1 = 0.666666675$, $\alpha_2 = 1.333333307$ and $\alpha_3 = 2.000000413$.

The domain has been partitioned into only three elements as shown in Fig. 14, and the first 3 GFIFs were then extracted, taking R to be 0.9. The number of degrees of freedom, the relative error in energy norm (%), and the computed values of the three GFIFs are listed in Table 2. Of course, A_1^{FE} has to converge to 1, and A_2^{FE} and A_3^{FE}, have to converge to 0. We may see from Table 2 that the GFIFs converge strongly and obviously, although not monotonically. Our method yields solutions at p-level 2 or 3 that are within the range of precision normally needed in engineering computations.

We have plotted the relative error in energy norm, the relative error in energy and the relative error in A_1 on a log-log scale in Fig. 15. The convergence path of the GFIF A_1^{FE} follows closely that of the "energy", which is a behavior referred to as "super-convergence".

This problem clearly demonstrates the effectiveness and the super-convergent property of the proposed method for anisotropic materials.

Table 2. First 3 GFIFs for the scalar anisotropic problem

	$p=1$	$p=2$	$p=3$	$p=4$	$p=5$	$p=6$	$p=7$	$p=8$
DOF	4	11	21	34	50	69	91	116
$\|e\|_E(\%)$	29.07	14.84	10.06	7.45	5.83	4.74	3.96	3.39
A_1^{FE}	0.8976059	0.9855478	0.9846905	0.9959510	0.9955990	0.9976367	0.9985509	0.9984618
A_2^{FE}	0.0539073	0.0025256	0.0003571	0.0004857	1.3e-7	7.8e-5	0.0001106	2.8e-5
A_3^{FE}	1e-10	1e-10	1e-10	1e-10	1e-10	1e-10	1e-10	1e-10

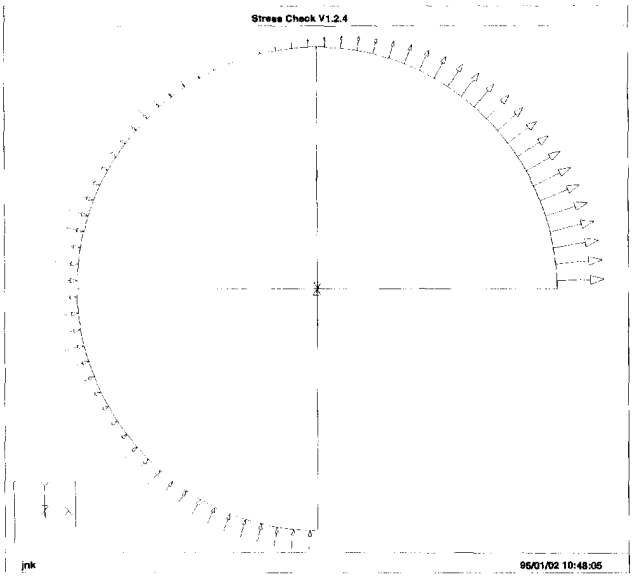

Fig. 14. F. E. mesh and boundary conditions for scalar problem 2.

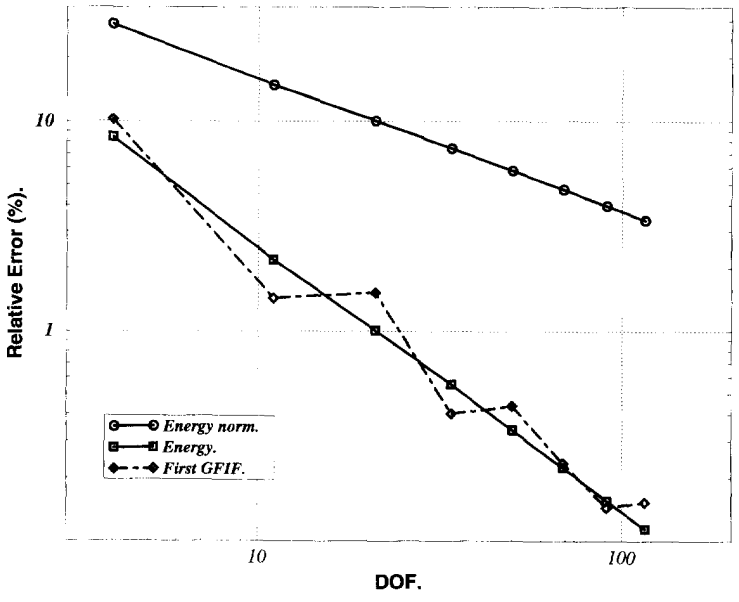

Fig. 15. Convergence of $\|e\|_E$, the energy ($\|e\|_E^2$), and A_1^{FE} for the scalar anisotropic problem.

5.3. *Scalar problem* 3: *results*

The performance of the modified Steklov method is demonstrated by Table 3 where we report the relative error of the first and second computed eigenvalues. A finite element mesh consisting of six elements, such that the inner elements have a radius of 0.15 has been

Table 3. Relative error (%) in first two eigenvalues ($\lambda_1^{EX} = 0.731691779$, $\lambda_2^{EX} = 1.268308221$)

	$p=1$	$p=2$	$p=3$	$p=4$	$p=5$	$p=6$	$p=7$	$p=8$
DOF	8	18	28	41	57	76	98	123
CPU†(sec)	0.19	0.07	0.13	0.26	0.45	0.75	1.4	2.24
$e_{\lambda_1}(\%)$	10.32	0.377	0.0069	7.0e-5	4.3e-7	1.0e-9	3.0e-11	1.0e-10
$e_{\lambda_2}(\%)$	-3.94	0.909	0.0270	4.4e-4	4.5e-6	7.9e-8	1.0e-10	1.0e-10

† Computations performed on a Silicon Graphics IRIS Indigo workstation (R3000, 24MB of RAM, SpecMark89 = 28).

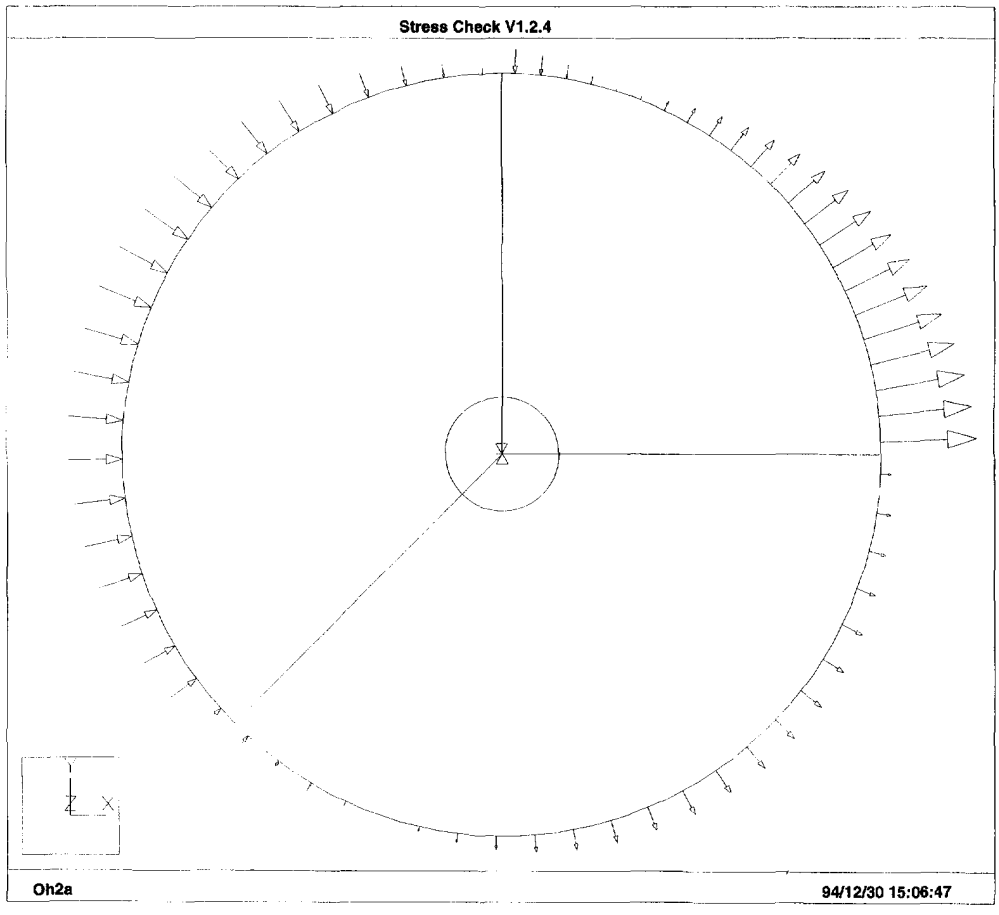

Fig. 16. F. E. mesh and boundary conditions for scalar problem 3.

used (see Fig. 16) together with the eigenvalues obtained by the modified Steklov method at $p = 8$, for computing the first two GFIFs A_1^{FE} and A_2^{FE}. These GFIFs, according to (15), have to converge to 1 as the number of degrees of freedom is increased. The number of degrees of freedom, the relative error in energy norm (%), the relative error in energy (%), the computed value of the GFIFs, and the relative error in GFIFs (%) are listed in Table 4 for $R = 0.6$. The data in Table 4 is plotted on a log-log scale in Fig. 17. It is seen that the rate of convergence of the GFIF is faster than the rate of convergence in the energy norm, and although not monotonic, is similar to the rate of convergence of the energy.

5.4. *Elastostatic problem* 1 : *results*

The eigenpairs were computed using the modified Steklov method resulting with $(\alpha_1)_{approx} = 0.5444837375$ and $(\alpha_2)_{approx} = 0.9085291893$ at $p = 8$. The eighteen-element mesh

Table 4. First two GFIFs for scalar problem 3 : two periodic isotropic material

DOF	$p=1$ 6	$p=2$ 18	$p=3$ 33	$p=4$ 54	$p=5$ 81	$p=6$ 114	$p=7$ 153	$p=8$ 198
$\|e\|_E(\%)$	73.68	10.52	8.47	1.28	0.75	0.51	0.41	0.34
$\|e\|_E^2(\%)$	54.28	1.11	0.717	0.0164	0.0056	0.0026	0.00168	0.001156
A_1^{FE}	0.82729	0.98729	0.99934	0.99956	0.99973	0.99990	0.99993	0.99994
A_2^{FE}	0.19937	1.03126	0.03587	1.00040	0.99939	1.000006	1.00004	0.999997
$100(A_1^{FE}-A_1)/A_1$	−17.27	−1.27	−0.065	−0.0434	−0.0273	−0.0103	−0.0067	−0.0059
$100(A_2^{FE}-A_2)/A_2$	−80.06	3.12	3.587	0.0405	0.0610	0.0005	0.0037	0.00030

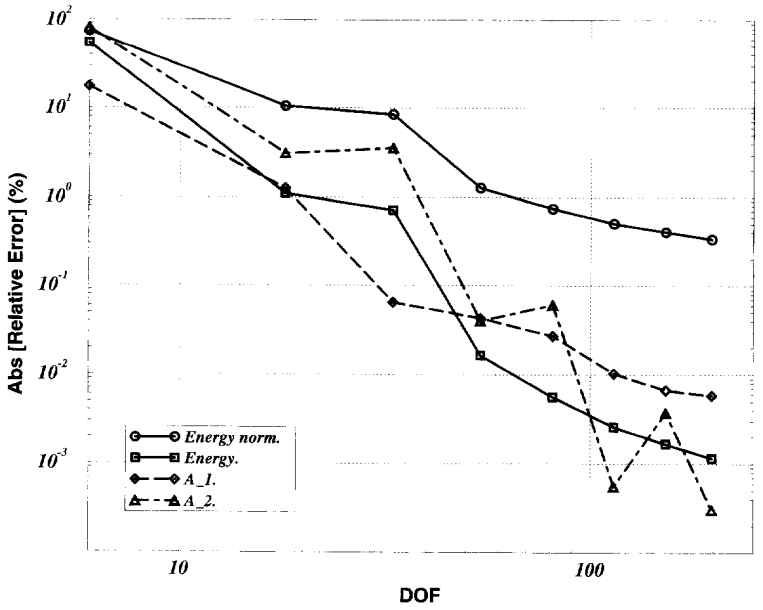

Fig. 17. Convergence of $\|e\|_E$, the energy ($\|e\|_E^2$), A_1 and A_2 for scalar problem 3.

shown in Fig. 18 in conjunction with the approximated eigenvalues were used for extracting A_1^{FE} and A_2^{FE}. Two radii, $R = 0.9$ and $R = 0.5$ were used for the integration path to illustrate the influence of R on the results. We define the normalized GSIFs:

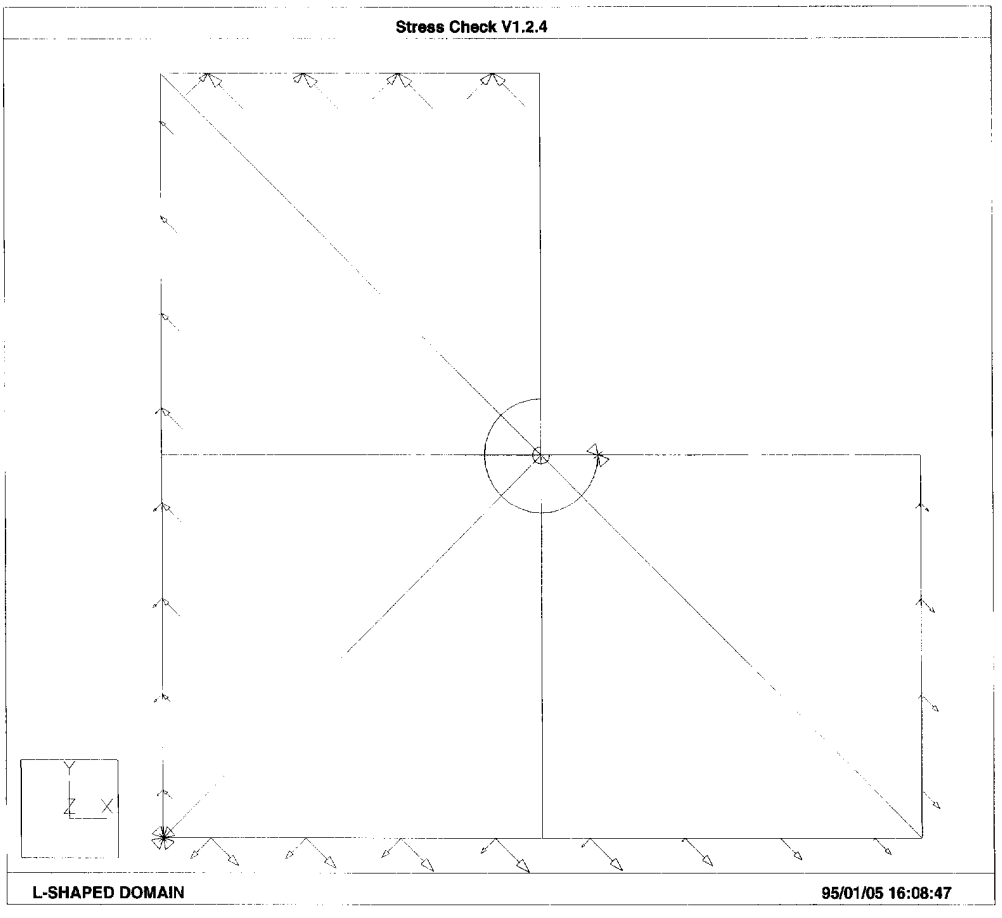

Fig. 18. Mesh design and boundary conditions for the L-shaped domain problem.

Table 5. First two GSIFs for the L-shaped isotropic material

		$p=1$	$p=2$	$p=3$	$p=4$	p = 5	$p=6$	$p=7$	$p=8$
	DOF	41	143	305	527	809	1151	1553	2015
	$\|e\|_E(\%)$	24.28	7.74	3.18	1.82	1.30	1.04	0.87	0.74
$R=0.9$	$\hat{A}_1$	0.895596	0.995697	0.998194	0.999131	0.999641	0.999670	0.999717	0.999750
	$100(A_1^{FE}-A_1)/A_1$	−10.44	−0.43	−0.18	−0.0869	−0.0359	−0.330	−0.0283	−0.0250
	$\hat{A}_2$	0.957941	0.997849	0.999954	0.999857	0.999984	0.999998	0.999991	0.999991
	$100(A_2^{FE}-A_2)/A_2$	−4.20	−0.215	−0.0046	−0.0143	−0.00157	−0.00017	−0.00091	−0.00087
$R=0.5$	$\hat{A}_1$	0.846893	0.972630	0.998131	1.000186	0.999505	0.999437	0.999597	0.999690
	$100(A_1^{FE}-A_1)/A_1$	−15.31	−2.74	−0.187	0.0186	−0.0494	−0.0563	−0.0403	−0.0309
	$\hat{A}_2$	0.941586	0.989872	0.998757	1.000180	1.000071	0.999976	0.999977	0.999990
	$100(A_2^{FE}-A_2)/A_2$	−5.84	−1.013	−0.1243	0.0180	0.0071	−0.00239	−0.00226	−0.00099

$$\hat{A}_i = A_i^{FE}/A_i \tag{44}$$

This way all normalized GSIFs are expected to converge to 1 (unless they are zero) as the number of degrees of freedom is increased. The number of degrees of freedom, the relative error in energy norm (%), the computed values of the normalized GSIFs, and the relative error in the GSIFs (%) are listed in Table 5. The absolute value of the relative error of A_1, A_2 for $R = 0.9$, the energy norm and the strain energy are plotted against the number of degrees of freedom on a log-log scale in Fig. 19. These results show that the relative error in strain energy and that of A_1 and A_2 are of comparable magnitude, and they converge at approximately the same rate, until the relative error drops below 0.1%. The path of integration has very little influence on the method's performance.

Incompressible materials: the same problem is analyzed in Yosibash and Szabó (1995a) for a nearly incompressible material (Poisson's ratio ν ranging from 0.499 to 0.4999999), where it is shown that the proposed methods are almost insensitive to ν up to $\nu = 0.4999999$.

5.5. *Elastostatic problem 2: results*

Numerical results for this crack problem have been reported in Yosibash and Szabó (1995a), where the performance of the present method was compared to the contour integral method. Herein, we show only the relative error in the energy norm, the relative error in the strain energy, and the absolute value of the relative error in the first two SIFs, plotted

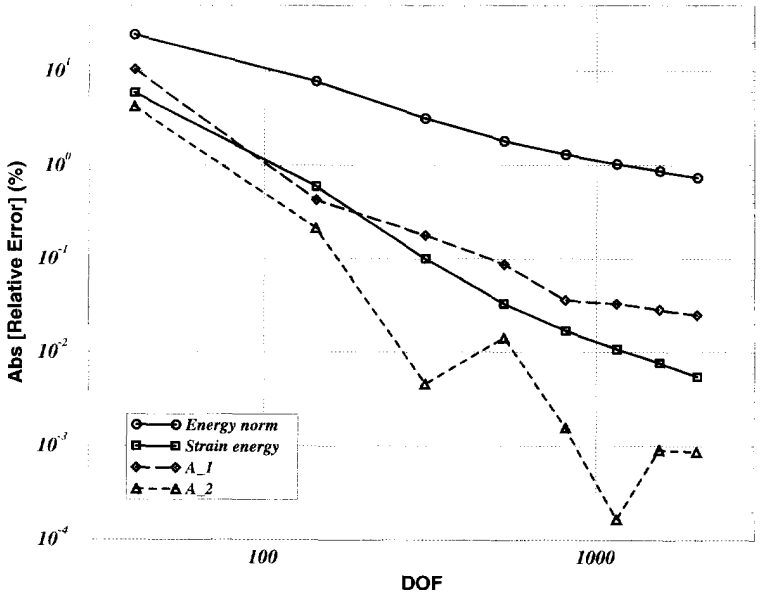

Fig. 19. Convergence of $|e|_E$, the strain energy ($\|e\|_E^2$), and $\hat{A}_1$, $\hat{A}_2$ for the L-shaped domain, $R = 0.9$.

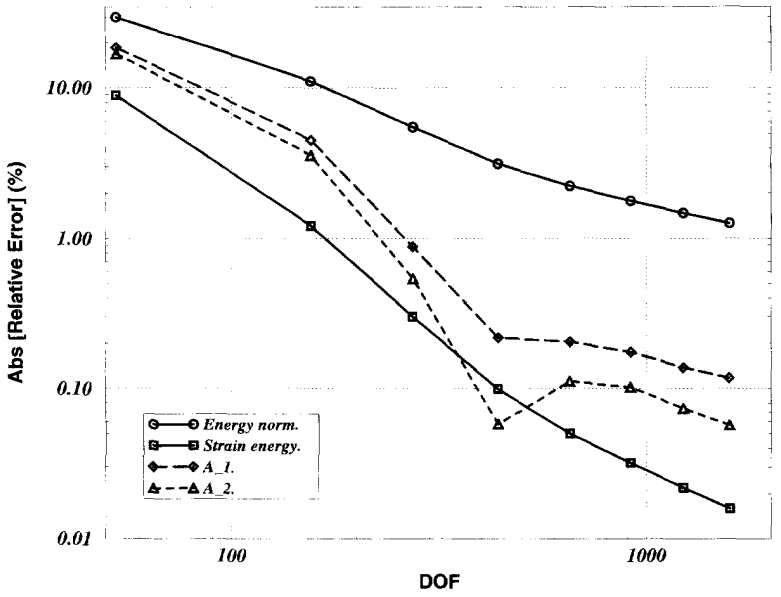

Fig. 20. Convergence of $\|e\|_E$, the strain energy ($\|e\|_E^2$), A_1^{FE} and A_2^{FE} for a crack in an isotropic material.

against the number of degrees of freedom on a log-log scale in Fig. 20. A mesh containing 16 elements was used in our computations. It is seen that the rate of convergence of the SIFs is faster than the rate of convergence of the solution measured in energy norm. The convergence patterns of the extracted SIFs by the proposed method are similar to these extracted by the contour integral method.

5.6. *Elastostatic problem* 3 : *results*

In our computations the approximated first eigenpair obtained by the modified Steklov method was used $(\alpha)_{approx} = 0.71117293326$. A finite element mesh consisting of two elements, such that the inner element has a radius of 0.15 has been used. (See Fig. 21.) The normalized GSIF is computed at $R = 0.6$. The number of degrees of freedom, the relative error in energy norm (%), the relative error in strain energy (%), the computed value of the normalized GSIF, and the relative error in GSIF (%) are listed in Table 6. The data in Table 6 is plotted on a log-log scale in Fig. 22. It is seen that the rate of convergence of the GSIF is faster than the rate of convergence in the energy norm, and although not monotonic, is similar to the rate of convergence of the strain energy.

5.7. *Elastostatic problem* 4 : *results*

The accuracy and convergence behavior of our method is demonstrated on the bi-material fracture mechanics problem shown in Fig. 8 where plane strain situation is assumed. The finite element mesh used is shown in Fig. 23. The outer radius of the domain has the radius of 1.5 and the two refined layers around the singular point have the radii $0.15 * 1.5$ and $0.15^2 * 1.5$. The polynomial level of the trial and test functions is increased over the shown mesh from 1 to 8. The stress intensity factors K_I and K_{II} in the expressions for the applied tractions are arbitrarily selected to be K. Again, we define the normalized stress intensity factors $\hat{K}_I$ and $\hat{K}_{II}$ as K_I^{FE}/K and K_{II}^{FE}/K, respectively.

Figure 24 shows the relative error in the energy norm, the relative error in strain energy and the absolute value of the relative error in the extracted SIFs as the number of degrees of freedom is increased on a log-log scale. The computations were done using an integration radius of 1.3. It is seen, as in the case of an isotropic material, that the existence of complex eigenpairs has no influence on the performance of the proposed method, and the SIFs converge to the exact values virtually as fast as the convergence rate of the strain energy. This example demonstrates that an accurate and efficient numerical solution of fracture

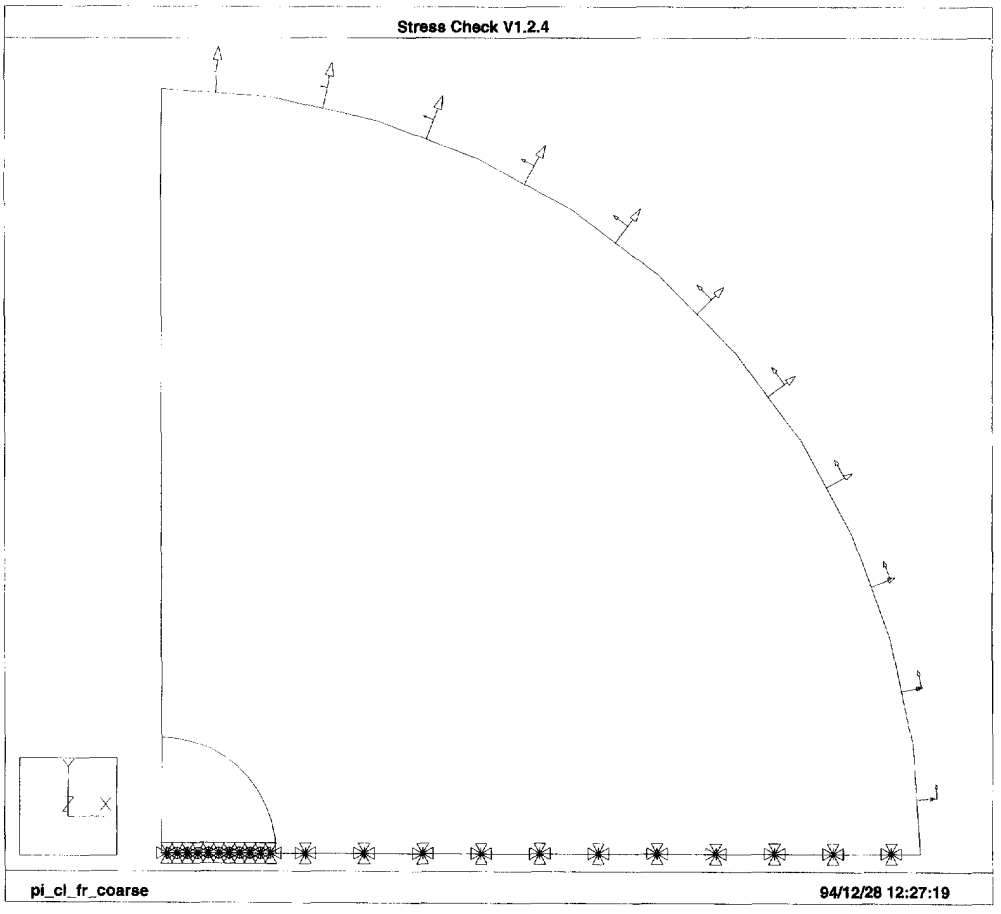

Fig. 21. F. E. mesh and boundary condition for elastostatic problem 3.

mechanics problems, even for such complicated situations as the crack at a bi-material interface, is possible.

5.8. *Elastostatic problem* 5 : *results*

The domain Ω is disretized by employing the finite element mesh shown in Fig. 25, having 1 radial layer graded geometrically toward the singular point with a grading factor 0.15. Using two terms in the series, and an integration path with $R = 0.8$, the error in the SIFs K_I and K_{II} converge as fast as the error in the potential energy. Figure 26 shows the relative error in the SIFs as the number of degrees of freedom is increased as compared to the relative errors in energy norm and potential energy.

5.9. *Elastostatic problem* 6 : *results*

The "deformed" configurations after imposing the rigid body motions are presented in Fig. 27. As expected, the computed SIFs are virtually zero; smaller than 10^{-10} at p-level = 8.

Table 6. First GSIF for the fixed-free 90° isotropic corner

DOF	$p=1$ 4	$p=2$ 12	$p=3$ 22	$p=4$ 36	$p=5$ 54	$p=6$ 76	$p=7$ 102	$p=8$ 132
$\|e\|_E(\%)$	16.25	9.16	3.29	2.20	1.64	1.31	1.08	0.91
$\|e\|_E^2(\%)$	2.64	0.84	0.11	0.0484	0.0256	0.0172	0.0117	0.0083
$\hat{A}_1$	0.90523	0.97633	1.00004	0.99920	0.99930	0.99960	0.99972	0.99977
$100(A_1^{FE}-A_1)/A_1$	−9.48	−2.37	0.0043	−0.0798	−0.0697	−0.0400	−0.0278	−0.0232

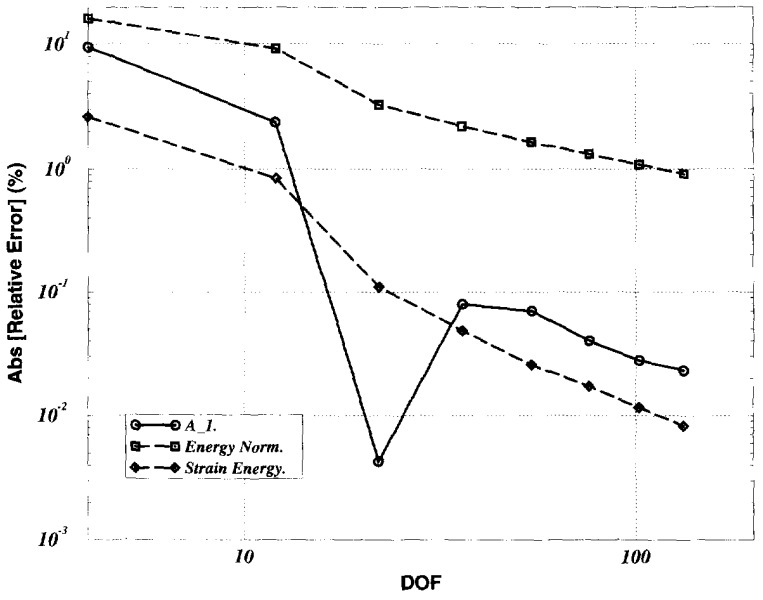

Fig. 22. Convergence of $\|e\|_E$, the strain energy ($\|e\|_E^2$), and A_1^{FE} for elastostatic problem 3.

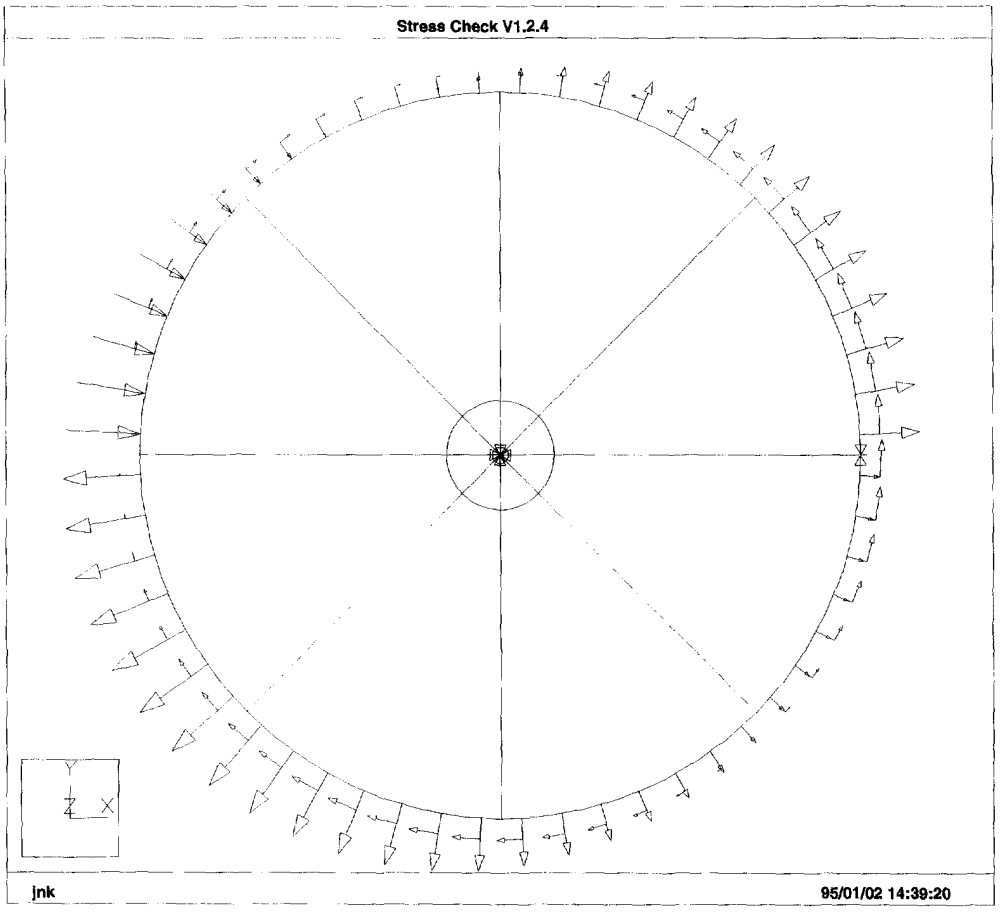

Fig. 23. Mesh design and boundary conditions for a crack at a bi-material interface.

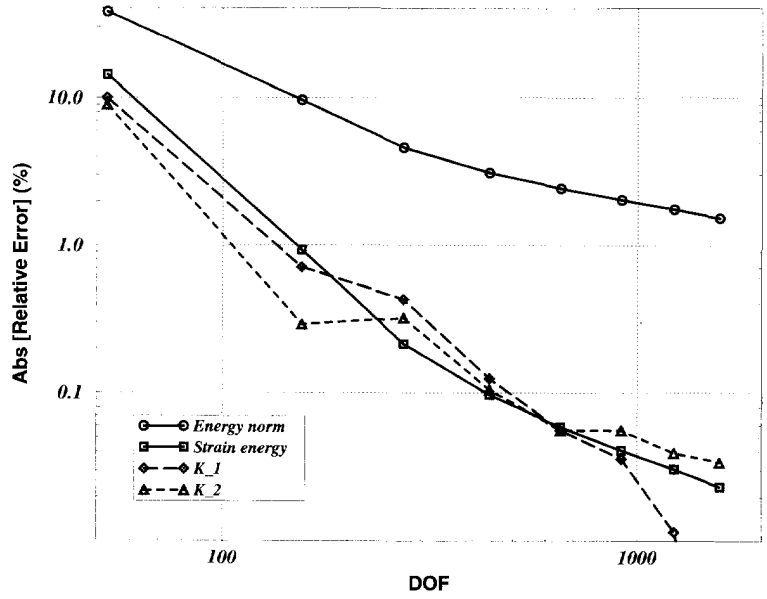

Fig. 24. Convergence of $\|e\|_E$, the strain energy ($\|e\|_E^2$), $\hat{K}_I$ and $\hat{K}_{II}$ for a crack at a bi-material interface.

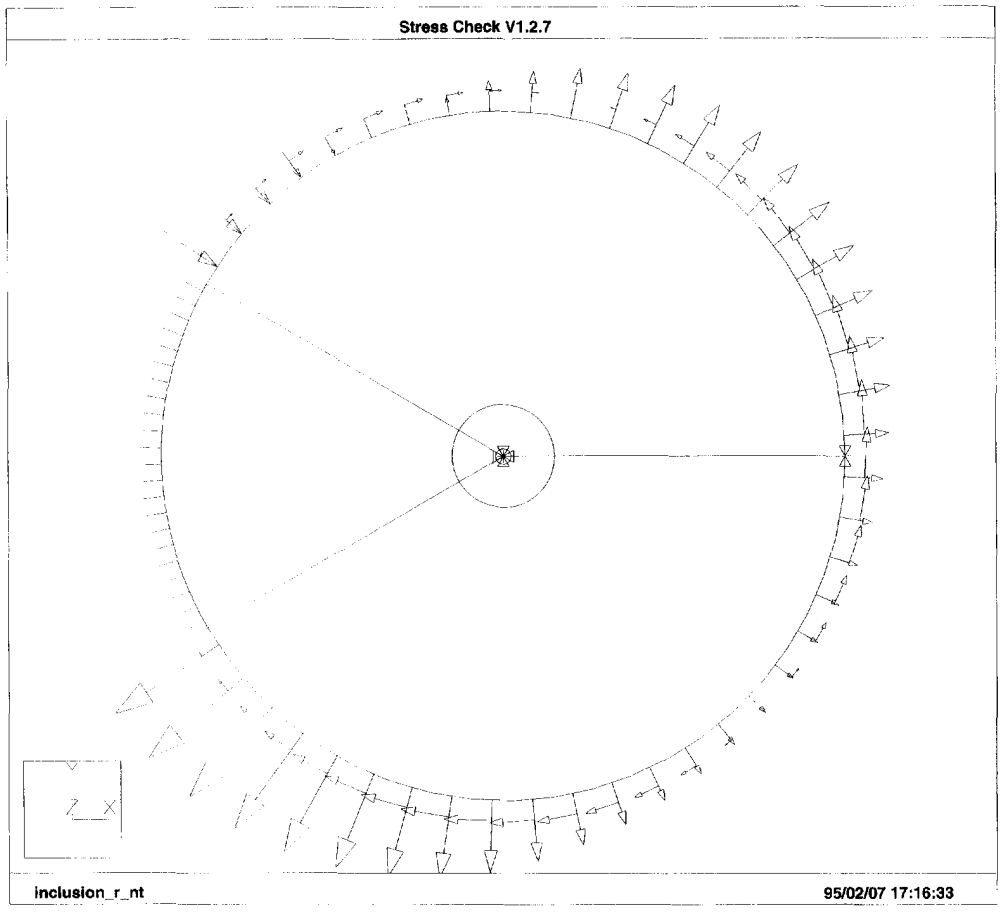

Fig. 25. Mesh and loading for elasticity inclusion problem.

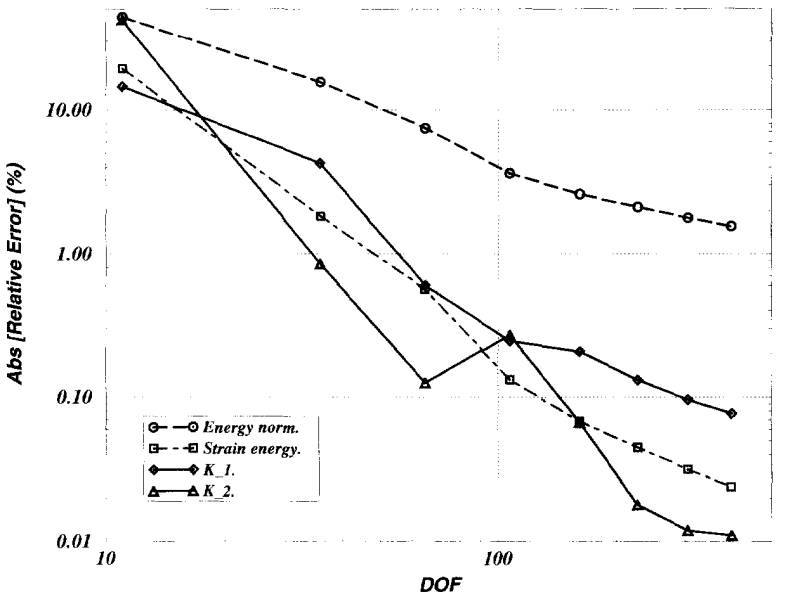

Fig. 26. Convergence of SIFs for elasticity inclusion problem.

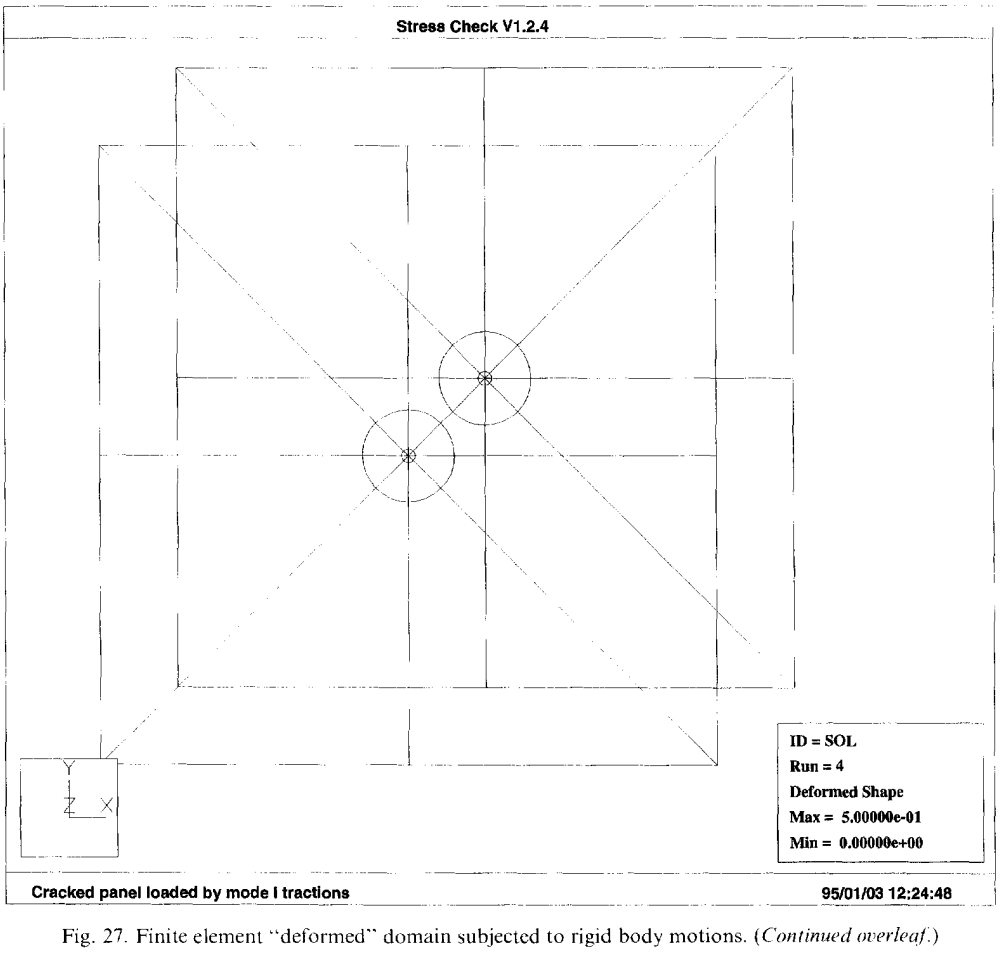

Fig. 27. Finite element "deformed" domain subjected to rigid body motions. (*Continued overleaf.*)

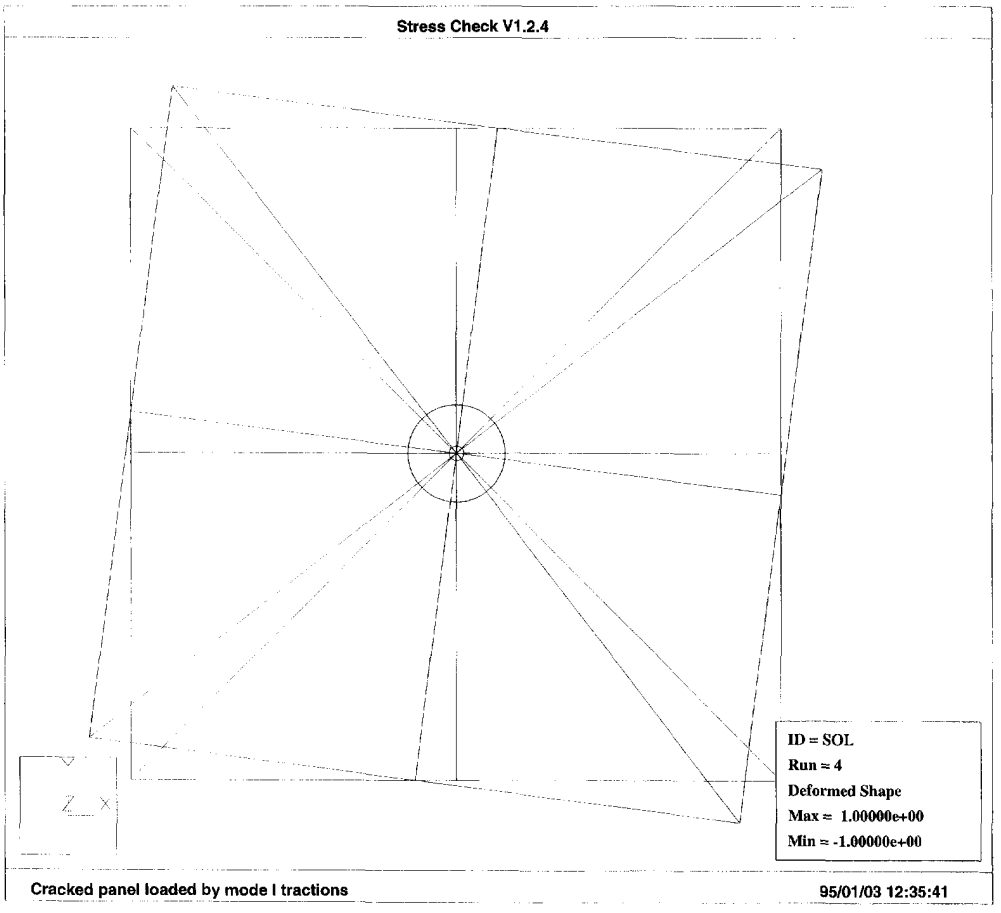

Fig. 27. (*Continued.*)

6. SUMMARY AND CONCLUSIONS

A set of benchmark problems representative of linear steady-state heat transfer and elastostatic models with singular points have been presented. The problems have been designed to include most types of singularities that occur in practical engineering problems. Their exact solutions (i.e., the eigenpairs and the GFIFs/GSIFs) are described in sufficient detail to allow reproduction. Importantly, we propose problems associated with anisotropic materials, wedge corners of different angles and materials, internal multi-material interfaces, and a case where power-logarithmic stress singularity is present in addition to the traditional crack tip singularities. This set of problems is intended to allow developers and users in this important field of fracture mechanics and failure initiation theory to assess the accuracy, robustness and efficiency of proposed numerical methods. They can be used for finding and correcting errors and weaknesses in numerical algorithms that compute eigenpairs and GFIFs/GSIFs.

Reliable and efficient numerical methods for the computation of eigenpairs and the coefficients of asymptotic expansion, the GFIFs/GSIFs, are of great practical importance because failure theories directly or indirectly involve these coefficients. These quantities are especially important for anisotropic materials or in locations where two or more materials are joined, because there is an increasing interest in composite materials and electronic packaging. The performance of new numerical methods, based on the p-version of the finite element method, was demonstrated by solving the benchmark problems. These methods provide both the eigenpairs and the GFIFs/GSIFs. Importantly, the methods are applicable to anisotropic materials, multi-material interfaces, and cases where the singularities are characterized by complex eigenpairs. New results on dissimilar wedges, perfectly bonded along all their common interfaces (multi-material internal interfaces), fixed-free corners,

and power-logarithmic stress singularities are reported herein for the first time. It is shown that the numerical methods yield results of high accuracy, are robust and efficient.

Acknowledgements—The writer gratefully acknowledges helpful advice and discussions with Professor Barna A. Szabó of Washington University in St Louis. The writer thanks Prof. J. P. Dempsey of Clarkson University, U.S.A. for bringing to his attention papers related to logarithmic stress singularities and singularities associated with anisotropic materials, and Dr Andre Noel of the CCM at Washington University in St Louis for his comments on the manuscript. The work reported herein was partially supported by the Air Force Office of Scientific Research under grant No. F49620-93-1-0173.

REFERENCES

Atluri, S. N. and Nakagaki, M. (1986). Computational methods for plane problems of fracture. In *Computational methods in the mechanics of fracture*, (ed. S. N. Atluri) Elsevier, Amsterdam, pp. 169–227.

Babuška, I. and Miller, A. (1984). The post-processing approach in the finite element method—Part 2: the calculation of stress intensity factors. *Int. J. Num. Meth. Engng* **20,** 1111–1129.

Banks-Sills, L. and Sherman, D. (1986). Comparison of methods for calculating stress intensity factors with quarter-point elements. *Int. J. Fract.* **32,** 127–140.

Chen, D.-H. (1994). Analysis of singular stress field around the inclusion corner tip. *Engng Frac. Mech.* **49,** 533–546.

Dempsey, J. P. (1995). Power-logarithmic stress singularities at bi-material corners and interface cracks. *J. Adhesion Sci. Tech.* **9,** 253–265.

Dempsey, J. P. and Sinclair, G. B. (1979). On the stress singularities in the plane elasticity of the composite edge. *J. Elasticity* **9,** 373–391.

Dempsey, J. P. and Sinclair, G. B. (1981). On the singular behavior at the vertex of a bi-material wedge. *Elasticity* **11,** 317–327.

Gregory, R. D. (1979). Green's functions, bi-linear forms, and completeness of the eigenfunctions for the elastostatic strip and wedge. *J. Elasticity* **9,** 283–309.

Hong, C. and Stern, M. (1978). The computation of stress intensity factors in dissimilar materials. *J. Elasticity* **8,** 21–34.

Lin, K. Y. and Mar, J. W. (1976). Finite element analysis of stress intensity factors for cracks at a bi-material interface. *Int. J. Fract.* **12,** 521–531.

Matos, P. P. L., McMeeking, R. M., Charalambides, P. G. and Drory, M. D. (1989). A method for calculating stress intensities in bimaterial fracture. *Int. J. Fract.* **40,** 235–254.

Murakami, Y. (1987). *Stress Intensity Factors Handbook*, Vols 1 and 2, Pergamon Press, New York.

Oh, H.-S. and Bubuška, I. (1992). P-version of the finite element method for the elliptic boundary value problems with interfaces. *Computer Meth. Appl. Mech. Engng* **97,** 211–231.

Rice, J. R. and Sih, G. C. (1965). Plane problems of cracks in dissimilar media. *Trans. ASME, J. Appl. Mech.* **32,** 418–423.

Stern, M. and Soni, M. L. (1976). On the computation of stress intensities at fixed-free corners. *Int. J. Solids Structures* **12,** 331–337.

Suo, Z. (1989). Mechanics of interface fracture. PhD thesis, Harvard University, Cambridge, Massachusetts, U.S.A.

Szabó, B. A. and Babuška, I. (1988). Computation of the amplitude of stress singular terms for cracks and reentrant corners. In *Fracture Mechanics: Nineteenth Symposium*, ASTM STP 969, ASTM, Philadelphia, pp. 101–124.

Szabó, B. A. and Babuška, I. (1991). *Finite Element Analysis*, John Wiley & Sons, New York.

Szabó, B. A. and Yosibash, Z. (1996). Numerical analysis of singularities in two-dimensions. Part 2: computation of the generalized flux/stress intensity factors. *Int. J. Num. Meth. Engng* **39,** 409–434.

Ting, T. C. T. (1986). Explicit solution and invariance of the singularities at an interface crack in anisotropic composites. *Int. J. Solids Structures* **22,** 965–983.

Whiteman, J. R. and Akin, J. E. (1979). Finite elements, singularities and fracture. In *The Mathematics of Finite Elements and its Applications III* (ed. J. R. Whiteman), Academic Press, London, pp. 35–54.

Williams, M. L. (1952). Stress singularities resulting from various boundary conditions in angular corners of plates in extension. *Trans. ASME, J. Appl. Mech.* **19,** 526–528.

Ying, X. (1986). A reliable root solver for automatic computation with application to stress analysis of a composite plane wedge. PhD thesis, Washington University, St Louis, Missouri, U.S.A.

Yosibash, Z. (1994). Numerical analysis of singularities and first derivatives for elliptic boundary value problems in two-dimensions. D.Sc. thesis, Sever Institute of Technology, Washington University, St Louis, Missouri, U.S.A.

Yosibash, Z. and Schiff, B. (1993). A superelement for two-dimensional singular boundary value problems in linear elasticity. *Int. J. Fract.* **62,** 325–340.

Yosibash, Z. and Szabó, B. A. (1995a). Generalized stress intensity factors in linear elastostatics. *Int. J. Fract.* **72,** 223–240.

Yosibash, Z. and Szabó, B. A. (1995b). Numerical analysis of singularities in two-dimensions. Part 1: computation of eigenpairs. *Int. J. Num. Meth. Engng* **38,** 2055–2982.

APPENDIX A. POWER-LOGARITHMIC STRESS SINGULARITY

The analytical conditions governing the occurrence of a power-logarithmic stress singularity, $\mathcal{O}(r^{\alpha-1}\ln r)$, are presented in Dempsey (1995), where it is shown that for a free-clamped wedge of a specific Poisson's ratio the

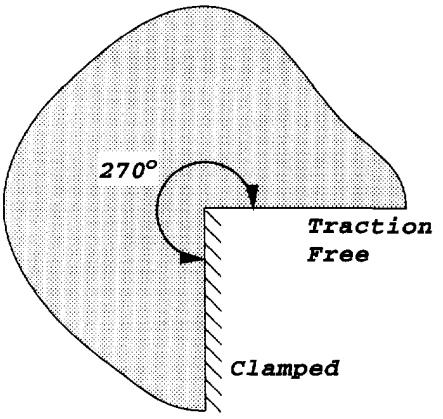

Fig. A.1. Free-clamped wedge exciting power-logarithmic stress singularity.

power-logarithmic stress singularity is excited. For a 270° free-clamped wedge (see Fig. A.1) in an isotropic material with a Poisson's ratio $\nu = 0.331046412$, the stress field contains power-logarithmic singularity, see Dempsey (1995, Table 1):

$$\sigma = A_1 r^{0.34254974-1}\mathbf{f}_1(\theta) + A_2 r^{0.34254974-1}\ln r\mathbf{f}_2(\theta) + \text{h.o.t.} \tag{A.1}$$

To demonstrate the robustness, in respect to power-logarithmic singularity types, of the proposed method, we present the first two eigenpairs obtained using the modified Steklov method. These are computed on a 4 element mesh. It is expected that the first two eigenvalues will collapse into a single one as the p-level (representing number of degrees of freedom) is increased, and the corresponding eigen-stresses will become identical. In Table A.1 we summarize the first two computed eigenvalues obtained as the p-level is increased from 1 to 8. The first and second eigen-stresses σ_x and σ_y for p-levels 3 and 8 are shown in Figs A.2–A.5. As observed, the first two eigenvalues and eigen-stresses collapse into one as the number of degrees of freedom is increased, indicating the presence of the power-logarithmic stress singularity.

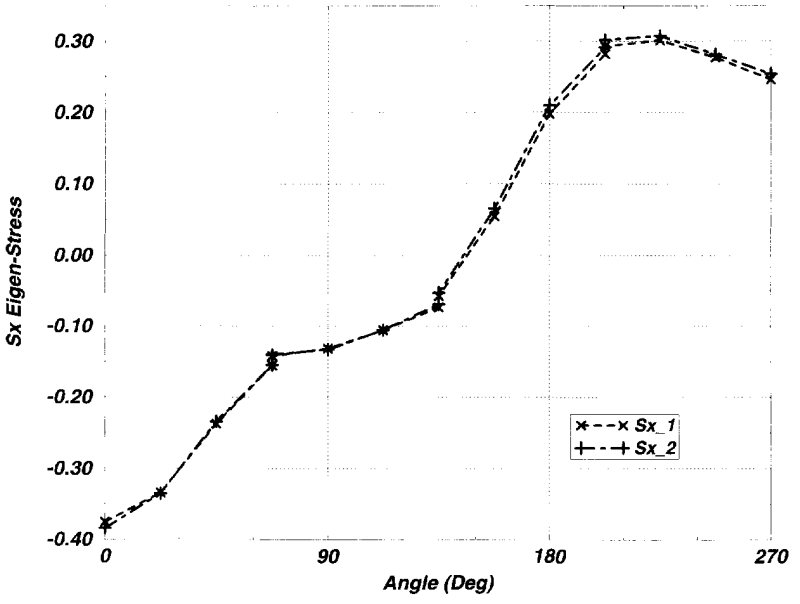

Fig. A.2. First and second σ_x eigen-stresses at $p = 3$.

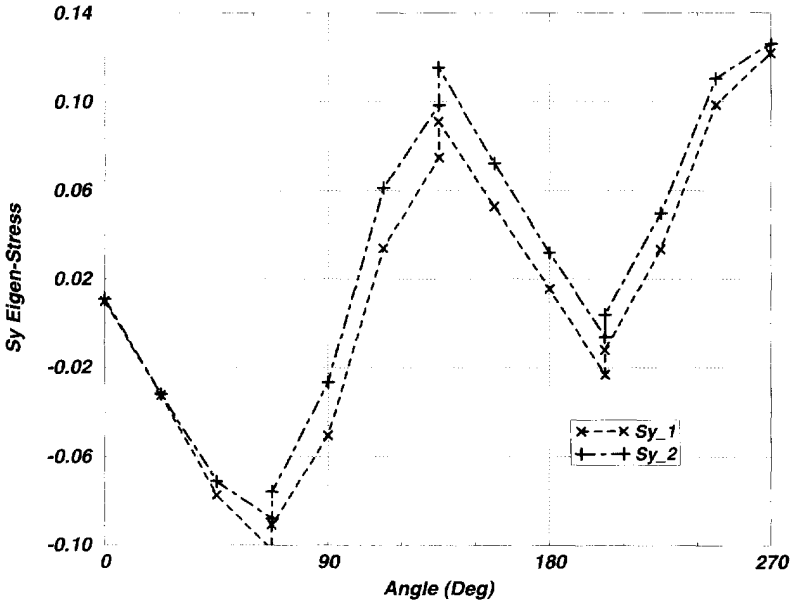

Fig. A.3. First and second σ_y eigen-stresses at $p = 3$.

Table A.1. First two computed eigenvalues which have to collapse to a single value $\alpha_1^{EX} = 0.34254974$

	$p = 1$	$p = 2$	$p = 3$	$p = 4$	$p = 5$	$p = 6$	$p = 7$	$p = 8$
DOF	20	46	72	106	148	198	256	322
α_1^{FE}	0.29603441	0.31881456	0.33848389	0.34183181	0.34254967†	0.34251766	0.34253064	0.34254449
α_2^{FE}	0.38225179	0.36605285	0.34658798	0.34326833	0.34254967†	0.34258184	0.34256885	0.34255499

† Complex conjugates with imaginary part $\pm 0.000108i$.

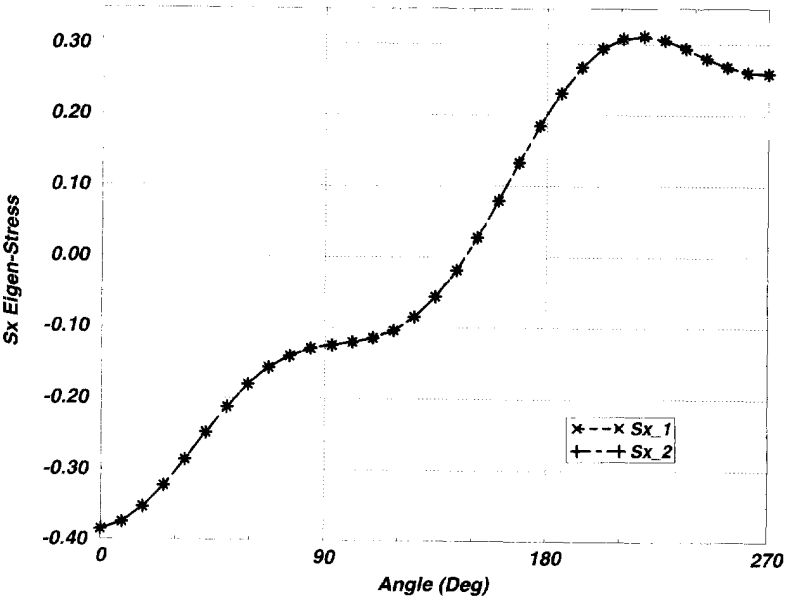

Fig. A.4. First and second σ_x eigen-stresses at $p = 8$.

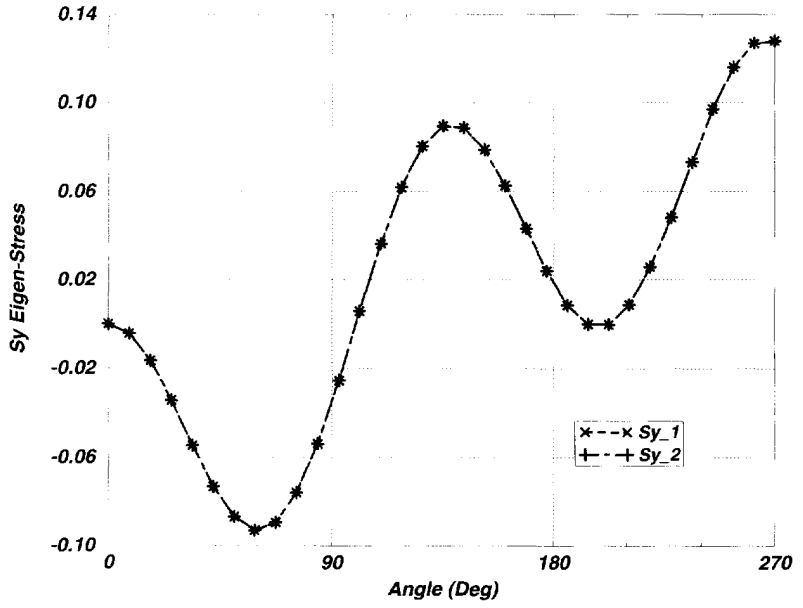

Fig. A.5. First and second σ_y eigen-stresses at $p = 8$.